SATURATED LIQUID VISCOSITY AND SURFACE TENSION OF ALTERNATIVE REFRIGERANTS[1]

A. P. Fröba[2], S. Will[3], and A. Leipertz [2,4]

---

[1] Paper presented at the Fourteenth Symposium on Thermophysical Properties, June 25-30, 2000, Boulder, Colorado, U.S.A.

[2] Lehrstuhl für Technische Thermodynamik (LTT), Friedrich-Alexander-Universität Erlangen-Nürnberg, Am Weichselgarten 8, D-91058 Erlangen, Germany

[3] Technische Thermodynamik / Wärme- und Stofftransport (TTWSt), Universität Bremen, FB4, Badgasteiner Straße 1, D-28359 Bremen, Germany

[4] Author to whom correspondence should be addressed.

ABSTRACT

Light scattering by thermally excited capillary waves on liquid surfaces or interfaces can be used for the investigation of viscoelastic properties of fluids. In this work, we carried out the simultaneous determination of the surface tension and the liquid kinematic viscosity of some alternative refrigerants by surface light scattering (SLS) on a gas-liquid interface. The experiments are based on a heterodyne detection scheme and signal analysis by photon correlation spectroscopy PCS. R23 (Trifluoromethane), R32 (Difluoromethane), R125 (Pentafluoroethane), R143a (1,1,1-Trifluoroethane), R134a (1,1,1,2-Tetrafluoroethane), R152a (1,1-Difluoroethane), and R123 (2,2-Dichloro-1,1,1-trifluoroethane) were the refrigerants investigated at saturation conditions over a wide temperature range from 233 K up to the critical point. It is estimated that the uncertainty of the present surface tension data for the whole temperature range is smaller than ± 0.2 $mN \cdot m^{-1}$. For temperatures of up to about 0.95 T_c the kinematic viscosity of the liquid phase could be obtained with an absolute accuracy of better than 2%. For the highest temperatures studied in this work measurements for the kinematic viscosity exhibit a maximum uncertainty of about ± 4 %. Viscosity and surface tension data are represented by a polynomial function of temperature and by a van der Waals-type surface tension equation, respectively. The results are discussed in detail in comparison with literature data.

KEY WORDS: dynamic light scattering; refrigerants; surface light scattering; surface tension; viscosity.

1. INTRODUCTION

The method of dynamic light scattering (DLS) for the determination of thermophysical properties of transparent fluids distinguishes itself by contactless operation and the possibility of determining a variety of properties close to thermodynamic equilibrium [1, 2]. Directly accessible properties comprise thermal diffusivity, speed of sound, sound attenuation and binary mass diffusion coefficient. By seeding fluids with spherical particles of known size it is also possible to obtain values for the particle diffusion coefficient and, hence, for the dynamic viscosity. The simultaneous determination of kinematic viscosity and surface tension is possible by applying the method of dynamic light scattering to fluid surfaces [3, 4], which may be denoted as surface light scattering (SLS). With this technique, the time-resolved analysis of light scattered by microscopic fluctuations of the liquid surface provides information on the desired quantities without the need of applying any external gradients.

In the present work the SLS method has been applied to various refrigerants. After a short introduction into the technique the experimental set-up is briefly described (details can be found elsewhere [5, 6]). In the main part of the paper, results for the surface tension and the liquid kinematic viscosity of R23, R32, R125, R143a, R134a, R152a and R123 under saturation conditions are discussed in comparison with recent literature data.

2. PRINCIPLE OF SURFACE LIGHT SCATTERING (SLS)

Liquid surfaces in macroscopic thermal equilibrium exhibit surface waves that are caused by the thermal motion of molecules and that are quantised in so-called “ripplons” [7]. Based on a classical hydrodynamic approach thermally excited surface oscillations result in

typical amplitudes of about 10 nm and wavelengths of about 10 µm [8, 9]. In order to excite surface fluctuations work has to be done against the forces acting on a liquid surface. Due to the typically small values of the wavelengths and amplitudes capillary forces dominate, while gravitational forces can be neglected [10]. A thermally excited surface can be represented by a superposition of waves with different amplitudes x_q and wave vectors $\vec{q}$ [4]. For a particular surface mode with frequency a the time-dependent vertical displacement x of the surface to its flat equilibrium state at a given point $\vec{r}$ is given by

$$x(\vec{r},t) = x_q \exp[i(\vec{q}\vec{r} + at)] . \tag{1}$$

For the propagation of capillary waves on a vapor-liquid interface the complex frequency a of a certain surface mode can be represented in first order approximation by

$$a = w + iG \approx \left[\frac{s\,q^3}{r' + r''}\right]^{1/2} + i\,2q^2\,\frac{h' + h''}{r' + r''}, \tag{2}$$

where s is the surface tension, r' and r'' are the densities of the liquid phase and the vapor phase, respectively, h' and h'' are the dynamic viscosities of the liquid and the vapor phase, respectively. Furthermore, the real part in Eq. (2) represents the frequency w and the imaginary part the damping G of the surface mode.

Light interacting with this oscillating surface structure is scattered. The scattering geometry typically used for light scattering experiments on liquid surfaces is shown in Fig. 1,

where scattered light is observed near reflection. By the choice of the reflection angle d and the scattering angle Q_s the scattering vector $\vec{q}=\vec{k}_I'-\vec{k}_S'$ is determined and by this the wave vector and frequency of the observed surface vibration mode. Here, $\vec{k}_I'$ and $\vec{k}_S'$ denote the projections of the wave vectors of the reflected ($\vec{k}_I$) and scattered light ($\vec{k}_S$) in the surface plane, respectively.

In light scattering experiments the surface oscillations described result in a temporal modulation of the scattered light intensity, which contains information on the dynamics of the surface. Information about this processes can be derived by a temporal analysis of the scattered light using photon correlation spectroscopy (PCS). For heterodyne conditions, where the scattered light is superimposed with coherent reference light, the time correlation function for the analysis of surface fluctuations is described by [4]

$$G^{(2)}(t) = A + B\cos(wt)\exp(-t/t_C), \qquad (3)$$

where the correlation time t_C and the frequency w are identical with the time decay behavior ($G = 1/t_C$) and the frequency of the surface oscillations. *A* and *B* are experimental constants. The correlation function can thus be used for the evaluation of the desired properties surface tension and viscosity, see Eq. (2).

3. EXPERIMENTAL

The experimental set-up and the scattering geometry used are shown in Fig. 2. A frequency-doubled continuous-wave Nd:YVO_4-laser operated in a single mode with a

wavelength of l_0 = 532 nm is used as a light source. The laser power was about 200 mW when working far from the critical point and only a few mW near the critical region. For the observation of light scattered by surface waves the optical path has to be aligned in a way that the laser beam and the direction of detection intersect on the liquid-vapor interface in the measuring cell. The time-dependent intensity of the scattered light is detected by two photomultiplier tubes (PMTs) operated in cross correlation in order to suppress afterpulsing effects. The signals are amplified, discriminated, and fed to a stand-alone correlator with 256 linearly spaced channels operated with a sample time down to 200 ns. In contrast to the more commonly employed scattering geometry, as depicted in Fig. 1, due to signal and stability considerations the analysis of the scattered light takes place in direction of the incident laser beam. Light scattered on the liquid-vapor interface will be detected at a defined angle Q_S with respect to the incident laser beam. With the help of Snell's refraction law and simple trigonometric identities, the modulus of the scattering vector q can be deduced as a function of the easily accessible angle of incidence

$$q = \frac{2p}{l_0} \sin(Q_E) . \qquad (4)$$

For the measurement of the angle of incidence Q_E, the laser beam is first adjusted through the detection system consisting of two apertures (∅ 1 - 2 mm) at a distance of about 4 m. Then the laser beam is set to the desired angle. For the experiment the angle of incidence Q_E was set between 3.0 ° and 4.5 ° and was measured with a precision rotation table. The error in the

angle measurement has been determined to be approximately ± 0.005 °, which results in a maximum uncertainty of less than 1.0 % for the desired thermophysical properties.

According to an analysis of the manufacturer (Solvay Fluor und Derivate GmbH, Hannover) the refrigerant samples used had a purity of 99.7% for R125, 99.9% for R32, 99.98% for R134a, and 99.99% for R143a. The refrigerants R23, R152a, and R123 a have a minimum purity of 99.5%, 99.9%, and 99.8%, respectively, according to specifications of the manufacturer. All refrigerants were used without further purification.

For the present measurements, the samples were filled from the vapor phase in an evacuated cylindrical pressure vessel (volume ≈ 10 cm^3) equipped with two quartz windows (Herasil I, diameter 30 mm x 30 mm). The temperature regulation of the cell surrounded by an insulating housing was realized with electrical heating. For temperatures below room temperature the insulating housing was cooled down to about 10 K below the desired temperature in the sample cell by a lab-thermostat. The temperature of the cell was measured with two calibrated Pt-100 Ω resistance probes, integrated into the main body of the vessel, with a resolution of 0.25 mK using an AC bridge (Paar, MKT 100). The accuracy of the absolute temperature measurement was better than ± 0.015 K. The temperature stability during an experimental run was better than ± 0.002 K. For each temperature, typically six measurements at different angles of incidence were performed, where the laser was irradiated from either side with respect to the axis of observation in order to check for a possible misalignment. The measurement times for a single run were typically of the order of ten minutes down to one minute for the highest temperatures in this study.

4. RESULTS AND DISCUSSION

The quantity directly accessible in surface light scattering experiments is the ratio $\tilde{s} = s/(r' + r'')$ of the surface tension s to the sum of the densities of the liquid and vapor phase. Similarly, also the direct quantity $\tilde{n}$ obtained for the viscosity is determined by both vapor and liquid properties, i.e. $\tilde{n} = (h' + h'')/(r' + r'')$, where h' and h'' are the dynamic viscosities of the liquid and vapor phase, respectively. If appropriate reference data for the quantities of the vapor phase are not available the approximation $\tilde{n} \approx n'$ can be used, which relies on the neglect of vapor properties as compared with the respective liquid quantities, and thus yields an approximate kinematic liquid viscosity. An estimation based on reference data indicates that for the fluids under investigation this approximation would result in a systematic deviation from the exact kinematic viscosity value of about + 3% for temperatures not to close to the critical point (T/T_c < 0.9). For the highest temperatures studied in this work the systematic error caused by neglecting the influence of the vapor phase would increase up to - 10%. In the present work, however, data obtained for $\tilde{n}$ and $\tilde{s}$ by an exact solution of the equation of dispersion for surface waves, see Ref. 6, have been combined with available reference data for the dynamic viscosity of the vapor phase and density data for both phases to get the information about the surface tension s and liquid kinematic viscosity n'.

For the refrigerants R23, R32, R125, R143a, R134a, R152a, and R123 the results for the desired quantities from surface light scattering are summarized in Table I, Fig. 3, and Fig. 4. The listed data are average values of typically six independent measurements with different angles of incidence Q_E. Also listed in Table I are the quantity $\tilde{n}$ obtained for the viscosity directly from the experiment, and the values from literature used for data evaluation as

described above. In detail, data for the liquid and vapor density under saturation conditions are calculated for R23 from McLinden [11] and a manufacturer's program [12], for R32 and R125 from the work of Outcalt and McLinden [13], for R143a from Srinivasan and Oellrich [14], for R134a from an equation of state of Tillner-Roth and Baer [15], for R152a from an equation of state of Tillner-Roth [16], and for R123 from an equation of state given by Younglove and McLinden [17]. The information listed in Table I for the dynamic viscosity of the vapor phase under saturation conditions is adopted for R23 from Ref. 18, for R32 and R125 from Ref. 19, for R134a from Ref. 20, for R152a from Ref. 21, and for R123 from Ref. 22. As literature data for the dynamic viscosity of saturated vapor of R143a could not be found the values listed in Table I for this fluid are calculated theoretically according to a method given in Refs. 23 and 24. With this approach vapor viscosity data can normally be predicted within ± 10% for temperatures not too close to the critical point which is good enough to maintain a reasonable absolute accuracy of better than 2% for the liquid kinematic viscosity. This estimate for the uncertainty of our viscosity values is based both on the standard deviation of the measurement values and on the uncertainty of the vapor data needed for the determination of true liquid kinematic viscosity from the direct observable $\tilde{n}$. As it is true for many DLS applications [25], the standard deviation of individual measurements may be considered as a reasonable measure for absolute experimental uncertainty. In most instances, this value was clearly below 1%. Similar to the uncertainty of the estimated vapor viscosities for R143a considerable differences of up to 15% may be found for experimental data in the literature (see, e.g., the differences for R125 and R152a in Refs. 19, 26, and 27). Although the vapor data have a comparatively small influence on the final results for liquid viscosities

well away from the critical point, possible errors in vapor viscosities may result in an additional uncertainty of about 1% in the desired quantity liquid viscosity. For the highest temperatures studied in this work ($T/T_c > 0.95$) these uncertainies may contribute to an overall maximum uncertainty of kinematic viscosity of about ± 4 %. In a similar way the uncertainty for the surface tension may be estimated. For the whole temperature range studied the standard deviation of individual measurements was clearly below ± 0.2 $mN \cdot m^{-1}$, and although the accuracy of density data is of course far better that those of viscosity data, some uncertainty is also introduced through the limited accuracy of the available density data. Yet in combination, a value of 0.2 $mN \cdot m^{-1}$ may be regarded as a fair estimate for the total uncertainty of the surface tension.

While a simple or modified Andrade-type equation may well represent the dynamic viscosity not too close to the critical point and some authors have simply adopted this approach for the kinematic viscosity, this type of equation fails to reasonably represent the kinematic viscosity for the whole temperature range studied in the present investigation. Thus we have chosen an empirical polynomial approach,

$$n' = \sum_{i=0}^{3} n'_i \left(\frac{T}{K} \right)^i \qquad (5)$$

in order to represent our experimental viscosity data, where the coefficients are given in Table II. Here, also the standard deviations of our data relative to those calculated by Eq. (5) are listed. The residuals of the experimental data from the fit are smaller than the standard deviation of the individual measurements.

The experimental data for the surface tension can be well represented by a van der Waals-type surface tension equation of the form

$$\sigma = \sigma_0 \left(1 - \frac{T}{T_c}\right)^n , \tag{6}$$

where T and T_c denote the temperature and the critical temperature, respectively. In Eq. (6), σ_0 and n are fit parameters, which are given in Table III and determined from our experimental results by least-squares fits. The value of the exponent n is obviously not constant for all refrigerants, which is in good agreement to former measurements [28] where n varies between 1.20 and 1.26. The critical temperatures for the refrigerants listed in Tab. III were adopted from the corresponding references used to calculate the information about the vapor and liquid density under saturation conditions [11-17]. The present correlations, according to Eq. (6), reproduce the experimental values of the surface tension for all refrigerants investigated with a root mean square deviation of better than 0.1 $mN \cdot m^{-1}$.

In the following, our data for liquid kinematic viscosity and surface tension are discussed for all substances investigated. As in most cases no generally accepted reference correlations exist and in order to provide consistent graphs relative deviations between our results and literature values are plotted using our respective correlations of Eqs. (5) and (6) as a basis. In Fig. 5-18 the exemplarily depicted error bars represent the standard deviation of the individual measurements.

4.1. Kinematic Viscosity

R23

In Fig. 5 the viscosity for R23 is compared with data given by Geller [18], who reports an uncertainty of 3-4% for values on the saturation line, and with measurements by Phillips and Murphy [29], which are part of a survey study of many refrigerants by the use of a capillary viscometer. Figure 5 also includes data predicted by Latini et al. [30], which are based on molecular constants and the critical parameters. Data for the saturated liquid density from the work of McLinden [11] have been used for the conversion of the data given in Refs. 18 and 30 from dynamic to kinematic viscosity. As it can be seen from Fig. 5 there is a large disagreement between the different data sets, where our data from surface light scattering seem to form the center.

R32

Data for the viscosity of R32 included in Fig. 6 comprise, beside the prediction by Latini et al. [30], measurements of Ripple and Matar [31] and of Sun et al. [32], which were both performed by capillary viscometers with stated maximum uncertainties of ± 5% and ± 3%, respectively. Also shown are measurements by Heide [33], which were performed by a falling-ball viscometer with a claimed uncertainty of 4 μPa·s, and measurements by Oliveira and Wakeham [19], which were obtained by a vibrating-wire viscometer with an estimated uncertainty of ± 0.6%. In Fig. 6 the depicted correlation of Grebenkov et al. [34] is based on experimental values of the falling-cylinder method, for which an uncertainty of less than ± 2.8% is stated. Finally, saturated liquid viscosity values as predicted by Sagaidakova et al. [35] and

a correlation by Assael et al. [36] have been included, which is based on experimental values from a vibrating wire instrument with an uncertainty of ± 0.5%. For the conversion of the data in Refs. 30, 34, 35, and 36 from dynamic to kinematic viscosity, density data from the equation of state from Outcalt and McLinden [13] have been used. Furthermore, vapor pressure data from this work were used for the calculation of the correlation given in Ref. 36. In the following discussion for R32 one must bear in mind that for our values only an accuracy of about of ± 5% could be achieved, mainly founded in a comparatively poor standard deviation of our measurements. This is due to the fact that R32 was the first refrigerant investigated in our lab with an initial version of the SLS instrument, and only after some improvements, mainly in the stability of the experimental set-up, the accuracy of better than ± 2% as stated for the other refrigerants could be achieved. Within the temperature range from 233 K to 293 K, however, our viscosity data for R32 agree with the reference data within the combined uncertainties, with the exception of the prediction of Sagaidakova et al. [35]. For temperatures below 300 K the average deviation of our data from the correlation of Grebenkov et al. [34] is 3.1 %. Yet, the situation becomes reversed for the higher temperature range. In this region, there is a positive deviation from the data given by Oliveira and Wakeham [19], Sun et al. [32], and Heide [33], whereas except for the highest temperature point agreement between our data and values of Sagaidakova et al. [35] is found.

R125

Values for the kinematic viscosity of liquid R125 under saturation conditions are compared in Fig. 7 with data by Oliveira and Wakeham [19], Latini et al. [30], Ripple and Matar [31], Sun

et al. [32], Heide [33], and Assael et al. [36]. Additionally included are measurements by Diller and Peterson [37], which were performed by a torsional crystal viscometer with an estimated precision of ± 3%, and data of Wilson et al. [38], which were determined by measuring the pressure drop of the fluid as it passed through a capillary at a known volumetric flow rate with a stated accuracy of ± 2%. These viscosity measurements were performed at 28 and 34 bar and are expected to be slightly higher than viscosities at saturation. Again, data for the saturated liquid density and vapor pressure from the work of Outcalt and McLinden [13] have been used for the conversion of the data given in Refs. 30, 36, and 38 from dynamic to kinematic viscosity. As it can be seen from Fig. 7, for temperatures between 220 and 300 K the depicted reference data with the exception of the prediction by Latini et al. [30], which crosses all other data, seem to define two bands. For temperatures up to 323 K our values are in good agreement with the data given by Ripple and Matar [31], Heide [33], Assael et al. [36], and Diller and Peterson [37]. In contrast, for low temperatures a systematic negative deviation from our values can be found for the data given by Oliveira and Wakeham [19] and Sun et al. [32]. In approaching the critical point these two data sets come closer to our data yet after crossing our data between 300 and 310 K they show a systematic positive deviation up to 63% for the highest temperatures studied in this work. This behavior is reflected in Oliveira's and Wakeham's data themselves, as the dynamic viscosity approaches a constant value and surprisingly decreases with increasing temperature, which cannot be explained by a critical enhancement at this distance from the critical point. For this range also the data given by Heide [33] and Diller and Peterson [37] show a systematic positive deviation of 31% and 12%, respectively, which is clearly outside the nominal combined uncertainties. Although a

definite reason for this behavior cannot be given yet, it is also obvious that most methods for viscosity measurements show a drastically worse performance in the neighborhood of the critical point, which makes a judgement on various data sets in this region a delicate problem.

R143a

At present, only two experimental data sets are available in literature for the saturated liquid viscosity of R143a. These are measurements of Heide [33], which were performed by a falling-ball viscometer, and of Kumagai and Takahashi [39], which were obtained by a capillary viscometer with an estimated error of less than 0.5%. In Fig. 8 experimental data from Refs. 33 and 39 and a prediction by Latini et al. [30] are compared with respect to our data. For the conversion of the prediction of Ref. 30 from dynamic to kinematic viscosity, density data from the work of Srinivasan and Oellrich [14] have been used. With the exception of few points at low temperatures (T < 290 K), reference data for R143a are very discordant. The data given by Kumagai and Takahashi [39] show an increasing positive deviation from our values with increasing temperature. In contrast, for the data given by Heide [33] an increasing negative deviation in respect of our data can be found at first with increasing temperature. Approaching the critical point the data from Ref. 33 cross our data and show a systematic positive deviation of 19% for the highest temperature.

R134a

Values for the kinematic viscosity of liquid R134a under saturation conditions are compared in Fig. 9 with data by Latini et al. [30], Ripple and Matar [31], Heide [33], Grebenkov et al.

[34], Assael et al. [36], and Kumagai and Takahashi [39]. The methods and their respective accuracies have already been discussed in context with R32 and R125, see above. Furthermore, data by Diller et al. [40], which were obtained by a torsional crystal viscometer, are included in Fig. 9. For this method an estimated precision of ± 3% is stated in Ref. 37. A comparison is also made with measurements by Oliveira and Wakeham [41], which have been carried out in a vibrating-wire viscometer with an overall accuracy of ± 0.6%. Finally, an equation for the viscosity of R134a by Krauss et al. [20] is included in Fig. 9, which has been obtained through a theoretically based, critical evaluation of available experimental data and where the uncertainty due to the inconsistencies between the experimental data sets cannot be better than ± 5%. For the conversion of the correlation by Assael et al. [36] and of the prediction by Latini et al. [30] from dynamic to kinematic viscosity, density data from the equation of state of Tillner-Roth and Baer [15] have been used. As it can be seen form Fig. 9 within the combined uncertainty good agreement between our data and those of Ripple and Matar [31], Grebenkov et al. [34], Assael et al. [36], and Oliveira and Wakeham [41] can be found. Furthermore, with the exception of the highest temperature point there is agreement of our data with the data set given by Kumagai and Takahashi [39]. The deviations between our measurements and the data set of Diller et al. [40] are partly larger than 6%, which exceeds the combined estimated uncertainties

R152a

Besides with data from the already mentioned Refs. 30, 33-36, and 39, see discussion above for R32, R125, and R134a, values for the kinematic viscosity of saturated liquid R152a are

compared in Fig. 10 with experimental data by van der Gulik [27] obtained by means of a vibrating-wire viscometer where the accuracy of the measurements is estimated to be ± 0.5%. Also, an equation for the viscosity of R152a by Krauss et al. [21] is depicted in Fig. 10, based on reliable, carefully selected data sets. For the conversion of the data of Refs. 30, 35, and 36 from dynamic to kinematic viscosity, density data from the equation of state by Tillner-Roth [16] have been used. Figure 10 shows an excellent agreement between our data from surface light scattering and those given by Assael et al. [36] and Kumagai and Takahashi [39]. Within the combined uncertainties this statement also holds for the data given by Heide [33] and Sagaidakova et al. [35]. Furthermore, particularly good agreement with an average deviation of 0.75% can be found between our data and the prediction by Latini et al. [30]. For the viscosity equation given by Krauss et al. [21] and the experimental data by van der Gulik [27] at low temperatures (T < 250 K) a pronounced positive deviation from our values can be recognized, which exceeds the combined uncertainties by far. Discrepancies in the low temperature range (T < 260 K) can also be found for the data correlation given by Grebenkov et al. [34], which shows an increasing negative deviation from our values with decreasing temperature.

R123

For R123 a data comparison of our values with reference data, as shown in Fig. 11, comprises predicted values by Latini et al. [30] and experimental values of Kumagai and Takahashi [39] and Diller et al. [40]. Also included is a correlation given by Tanaka and Sotani [42] with a stated uncertainty of 3%, based on a critical evaluation of literature data.

For the conversion of the data given by Refs. 30 and 42 from dynamic to kinematic viscosity, density data from the equation of state by Younglove and McLinden [17] have been used. As is can be seen from Fig. 11, good agreement can be found between all experimental data sets. For temperatures between 250 and 350 K the correlation by Tanaka and Sotani [42] is in good agreement with the experimental values. In contrast, by extrapolating our viscosity values only a small way down to temperatures T < 250 K, an increasing positive deviation with decreasing temperature from the present work can be observed for the correlation by Tanaka and Sotani [42].

4.2. Surface Tension

R23

In Fig. 12 our values for the surface tension of R23 are presented in comparison to data by Heide [43], which were obtained by the differential capillary rise method, published in 1973, where for a single experimental run an error of 0.5% in respect of a surface tension value of 20 $mN \cdot m^{-1}$ is stated. Beside the measurement values also the correlation from Ref. 43 is shown based on a linear temperature dependence, which is not applicable over a wide temperature range. In contrast to this, in Fig. 12, valid over a wide temperature range up to the critical point, a correlation by Okada and Watanabe [44] is included, which is based on carefully examined data sets, where also the data from Ref. 43 have been taken into account. Due to the lack of reliable experimental data the uncertainty of the correlation given by Okada and Watanabe [44] is estimated to be within ± 0.3 $mN \cdot m^{-1}$. Finally, surface tension values as predicted by Le Neindre [45] have been included, where the amplitude of the surface tension

is calculated by generalized equations based on corresponding states. As it can be seen from Fig. 12, for the temperature range studied in the present work, agreement can be found within the combined uncertainties. By extrapolating our values for temperatures $T < 230$ K low positive as well as negative deviations appear, where our data from surface light scattering seem to form the center.

R32

In the following exclusively surface tension data obtained by the differential capillary rise method are compared with our results from surface light scattering. In Fig. 13, as far as available, both measurement values and the respective authors' correlation are depicted, where a van der Waals-type surface tension correlation is proposed in the most cases for the representation of the temperature dependence up to the critical point. In detail, the data shown for comparison are given by Heide [46], where the stated error in measuring the surface tension when neglecting possible density errors amounts to ≤ 1 % for a surface tension of 10 $mN \cdot m^{-1}$, and by Okada and Higashi [47], where the accuracy is estimated to be ± 0.2 $mN \cdot m^{-1}$. While information about the accuracy of the surface tension data presented in the work of Zhu and Lu [48] is not available, these authors state that most of their measured data fit a van der Waals-type surface tension correlation with relative deviations of less than 3%. For the data correlation given by Schmidt and Moldover [49] an accuracy of ± 0.15 $mN \cdot m^{-1}$ can be adopted, see Ref. 28. With the exception of the data correlation given by Heide [46] for temperatures $T < 250$ K our values for the surface tension of R32 agree with the other data sets within the combined uncertainties.

R125

Figure 14 shows the data comparison for the surface tension of R125, where the accuracies of the available reference data based on the differential capillary rise method have already been discussed in context with R32, see above. For R125 our data from surface light scattering seems to form one coherent band with the data given by Heide [46], Okada and Higashi [47], and Schmidt and Moldover [49].

R143a

For the surface tension of R143a only two experimental data sets are available in the literature. These are the data by Heide [46] and a data correlation by Schmidt et al. [50], obtained again with the differential capillary rise method with a relative uncertainty in the surface tension of less than 2 % for temperatures far from the critical point ($T/T_c < 0.8$). For data comparison Fig. 15 also includes a prediction by Srinivasan and Oellrich [14], where saturated liquid and vapor densities were used according to a method described in Ref. 51. On the basis of the experimental uncertainties of the different techniques no systematic deviations can be found for the surface tension of R143a.

R134a

For the surface tension of R134a a considerable number of data sets are available, which are all based on the differential capillary rise method. In detail in Fig.16 our values from surface light scattering are compared with data by Heide [46] and measurements by Chae et al. [52], for which an accuracy of $\pm$ 0.15 $mN \cdot m^{-1}$ can be adopted, see Ref. 28. Surface tension values

by Sufen et al. [53] were obtained with a stated uncertainty of ± 0.1 $mN \cdot m^{-1}$. For the data correlation given by Zhu et al. [54] no direct information about the uncertainty of surface tension can be found. The correlation given by Higashi and Okada [55] is based on surface tension measurements with an estimated uncertainty of ± 0.2 $mN \cdot m^{-1}$. Finally, Fig. 16 includes a correlation by Okada and Higashi [28], which is based on the evaluation of different data sets and which has been accepted in Annex 18 of IEA (International Energy Agency) as the international standard for the surface tension of R134a. The uncertainty of the correlation is estimated to be within ± 0.2 $mN \cdot m^{-1}$ for temperatures above 273 K, while the correlation is less reliable for temperatures below 273, because of the discrepancies of the underlying data sets. For R134a our data from surface light scattering show excellent agreement with the data given by Heide [46] and with the internationally accepted standard from Ref. 28. Also, agreement of our values is found with the other data sets within the combined, estimated uncertainty.

R152a

Data for the surface tension of R152a from surface light scattering are compared in Fig. 17 with data by Heide [46], Okada and Higashi [47], Sufen et al. [53] and Higashi and Okada [55]. For information about the accuracies of these reference data see discussion above for R32 and R134a. Furthermore, in Fig. 17 a correlation by Chae et al. [56] is included, which is based on the differential capillary rise method and for which an accuracy of ± 0.15 $mN \cdot m^{-1}$ is adopted, see Ref. 28. Additionally from Ref. 28, a correlation with an accuracy of ± 0.2 $mN \cdot m^{-1}$ by Obata is adopted, which represents values of the single capillary

and differential capillary rise method. As it can be seen from Fig. 17, for temperatures between 250 K and 350 K the data sets given by Heide [46], Sufen et al. [53], and Chae et al. [56] show some differences to our data, which are outside the combined uncertainty, while good agreement can be found with the data given by Obata from Ref. 28, Okada and Higashi [47], and Higashi and Okada [55].

R123

For data comparison of the surface tension of R123 Fig. 18 comprises, beside the data reported by Chae et al. [52], a correlation by Higashi and Okada [55], which is based on experimental values of both the differential capillary rise method and the vertical plate method, where the uncertainties of the surface tension measurements were estimated to be ± 0.2 $mN \cdot m^{-1}$ and ± 0.4 $mN \cdot m^{-1}$, respectively. In addition, Fig. 18 includes the correlation accepted as the international standard for the surface tension of R123 in Annex 18 of IEA from the work of Okada and Higashi [28]. For the uncertainty of this correlation the same statement holds as in the case of R134a. Again, good agreement is found between our values and the international standard.

5. CONCLUSIONS

Our investigations have shown that surface light scattering on a horizontal liquid-vapor interface can be utilized for an efficient and reliable determination of viscosity and surface tension of refrigerants over a wide temperature range. Without any knowledge of vapor viscosity and density data the determination of the liquid kinematic viscosity is possible with an accuracy of typically ± 5 % over a wide temperature range, where the experimental uncertainty of the directly accessible quantity only contributes with about 1%. With the provision of approximate data for the vapor viscosity, however, the overall uncertainty can clearly be improved to a value of ± 2%. Measurements of the surface tension could be performed with an accuracy of better than ± 0.2 $mN \cdot m^{-1}$ over the total investigated temperature range for all refrigerants and show an excellent agreement with reference data. In future work we intend to apply surface light scattering also to mixtures of refrigerants.

ACKNOWLEDGEMENTS

The investigated refrigerants have been provided by Solvay Fluor und Derivate GmbH, Hannover. The authors gratefully acknowledge financial support for parts of this work by the Deutsche Forschungsgemeinschaft (DFG).

REFERENCES

[1] S. Will and A. Leipertz, in *Diffusion in Condensed Matter*, J. Kärger, P. Heitjans, and R. Haberlandt, eds. (Vieweg, Wiesbaden, 1999), pp. 219-244.

[2] A. Leipertz, *Fluid Phase Equil.* **125**:219 (1996).

[3] J. C. Earnshaw, *Appl. Opt.* **36**:7583 (1997).

[4] D. Langewin, *Light Scattering by Liquid Surfaces and Complementary Techniques*, Marcel Dekker, New York 1992.

[5] A. P. Fröba, S. Will, and A. Leipertz, *Appl. Opt.* **36**:7615 (1997).

[6] A. P. Fröba and A. Leipertz, *Int. J. Thermophys.*, submitted (2000).

[7] W. Brouwer and R. K. Pathria, *Phys. Rev.* **163**:200 (1967).

[8] R. H. Katyl and U. Ingard, *Phys. Rev. Lett.* **19**:64 (1967).

[9] R. H. Katyl and U. Ingard, *Phys. Rev. Lett.* **20**:68 (1968).

[10] D. Langewin and J. Meunier, in *Photon Correlation Spectroscopy and Velocimetry*, NATO Advanced Study Institutes Series, Series B: Physics, Vol. 23, H. Z. Cummins and E. R. Pike, Eds., (Plenum Press, New York, 1977), pp. 501-518.

[11] M. O. McLinden, *Int. J. Refrig.* **13**:149 (1990).

[12] Solvay Fluor & Derivate, SOLKANE® Refrigerant Software, Version 2.0 (1999).

[13] S. L. Outcalt and M. O. McLinden, *Int. J. Thermophys.* **16**:79 (1995).

[14] K. Srinivasan and L. R. Oellrich, Int. *J. Refrig.* **20**:332 (1997).

[15] R. Tillner-Roth and H. D. Baehr, *J. Phys. Chem. Ref. Data* **23**:657 (1994).

[16] R. Tillner-Roth, *Int. J. Thermophys.* **16**:91 (1995).

[17] B. A. Younglove and M. O. McLinden, *J. Phys. Chem. Ref. Data* **23**:731 (1994).

[18] V. Z. Geller, *Teplofiz. Svoistv. Veshch. Mat.* **15**:89 (1980).

[19] C. M. B. P. Oliveira and W. A. Wakeham, *Int. J. Thermophys.* **14**:1131 (1993).

[20] R. Krauss, J. Luettmer-Strathmann, J. V. Sengers, and K. Stephan, *Int. J. Thermophys.* **14**:951 (1993).

[21] R. Krauss, V. C. Weiss, T. A. Edison, J. V. Sengers, and K. Stephan, *Int. J. Thermophys.* **17**:731 (1996).

[22] H. Nabizadeh and F. Mayinger, *High Temp. High Press.* **24**:221 (1992).

[23] K. Lucas, *C. I. T.* **46**:157 (1974).

[24] R. C. Reid, J. M. Prausnitz, and B. E. Poling, The Properties of Gases and Liquids (McGraw Hill, New York, 1987).

[25] K. Kraft, M. Matos Lopes, and A. Leipertz, *Int. J. Thermophys.* **16**:423 (1995).

[26] M. J. Assael, A. A. Papadopoulos, and S. Polimatidou, Proc. *4th Asian Thermophysical Properties Conference* (Tokyo, 1995), Vol. 3, pp. 623-626.

[27] P. S. van der Gulik, *Int. J. Thermophys.* **16**:867 (1995).

[28] M. Okada and Y. Higashi, Proc. *International Conference CFCs, The Day After* (Padova, 1994), pp. 541-548.

[29] T. W. Phillips and K. P. Murphy, *J. Chem. Eng. Data* **15**:304 (1970).

[30] G. Latini, G. Passerini, and F. Polonara, *Fluid Phase Equil.* **125**:205 (1996).

[31] D. Ripple and O. Matar, *J. Chem. Eng. Data* **38**:560 (1993).

[32] L.-Q. Sun, M.-S. Zhu, L.-Z. Han, and Z.-Z. Lin, *J. Chem. Eng. Data* **41**:292 (1996).

[33] R. Heide, *DKV-Tagungsbericht 23*, (Leipzig, 1996), Vol. II.1, pp. 225-241.

[34] A. J. Grebenkov, V. P. Zhelezny, P. M. Klepatsky, O. V. Beljajeva, Yu. A. Chernjak, Yu. G. Kotelevsky, and B. D. Timofejev, *Int. J. Thermophys.* **17**:535 (1996).

[35] N. G. Sagaidakova, V. A. Rykov, and T. N. Tsuranova, *Kholod. Tekh.* **5**:59 (1990).

[36] M. J. Assael, L. Karagiannidis and S. K. Polimatidou, *Int. J. Thermophys.* **16**:133 (1995).

[37] D. E. Diller and S. M. Peterson, *Int. J. Thermophys.* **14**:55 (1993).

[38] L. C. Wilson, W. V. Wilding, G. M. Wilson, R. L. Rowley, V. M. Felix, and T. Chisolm-Carter, *Fluid Phase Equil.* **80**:167 (1992).

[39] A. Kumagai and S. Takahashi, *Int. J. Thermophys.* **12**:105 (1991).

[40] D. E. Diller, A. S. Aragon, and A. Laesecke, *Fluid Phase Equil.* **88**:251 (1993).

[41] C. M. B. P. Oliveira and W. A. Wakeham, *Int. J. Thermophys.* **14**:33 (1993).

[42] Y. Tanaka and T. Sotani, *Thermal conductivity and viscosity of 1,1-Dichloro-2,2,2-Trifluoroethane (HCFC-123)*, Progress report to the IEA Annex 18, Thermophysical properties of the environmentally acceptable refrigerants, Fukuoka, 1993.

[43] R. Heide, *Luft- und Kältetechnik* **9**:125 (1973).

[44] M. Okada and K. Watanabe, *Heat Transfer Japanese Research* **17**:35 (1988).

[45] B. Le Neindre and Y. Garrabos, Proc. *International Conference CFCs, The Day After* (Padova, 1994), pp. 549-556.

[46] R. Heide, *Int. J. Refrig.* **20**:496 (1997).

[47] M. Okada and Y. Higashi, *Int. J. Thermophys.* **16**:791 (1995).

[48] M.-S. Zhu and C.-X. Lu, *J. Chem. Eng. Data* **39**:205 (1994).

[49] J. W. Schmidt and M. R. Moldover, *J. Chem. Eng. Data* **39**:39 (1994).

[50] J. W. Schmidt, E. Carrillo-Nava, and M. R. Moldover, *Fluid Phase Equil.* **122**:187 (1996).

[51] K. Srinivasan, *Can. J. Chem. Eng.* **68**:493 (1990).

[52] H. B. Chae, J. W. Schmidt, and M. R. Moldover, *J. Chem. Eng. Data* **35**:6 (1990).

[53] D. Sufen, L. Zhigang, Y. Jianmin, and L. Deqing, Proc. *4th Asian Thermophysical Properties Conference* (Tokyo, 1995), Vol. 2, pp. 283-286.

[54] M.-S. Zhu, L.-Z. Han, Y.-D. Fu, J. Wu, and C.-X. Lu, Proc. *International Refrigeration Conference* (West Lafayette, 1992), Vol. 2, pp. 499-509.

[55] Y. Higashi and M. Okada, Proc. *18th International Congress of Refrigeration* (Montréal, 1991), Vol. 2, pp. 675-679.

[56] H. B. Chae, J. W. Schmidt, and M. R. Moldover, *J. Phys. Chem.* **94**:8840 (1990).

Table I: Viscosity and surface tension and of alternative refrigerants under saturation conditions.

T, K	$\tilde{n}$, $mm^2 \cdot s^{-1}$	h'', µPa·s	r', $kg \cdot m^{-3}$	r'', $kg \cdot m^{-3}$	n', $mm^2 \cdot s^{-1}$	s, $mN \cdot m^{-1}$
R23 (Trifluoromethane)						
233.15	0.1442	11.7	1273.9	30.5	0.1385	8.89
238.15	0.1367	12.0	1249.1	36.5	0.1311	8.12
243.15	0.1321	12.3	1223.4	43.6	0.1268	7.26
248.15	0.1254	12.6	1196.7	51.7	0.1202	6.44
253.15	0.1209	13.0	1168.7	61.1	0.1161	5.65
258.15	0.1151	13.4	1139.2	72.1	0.1106	4.89
263.15	0.1106	13.9	1108.0	85.0	0.1065	4.11
268.15	0.1042	14.4	1074.5	100.2	0.1005	3.42
273.15	0.0999	15.0	1038.2	118.4	0.0968	2.69
278.15	0.0924	15.7	998.1	140.5	0.0897	2.06
283.15	0.0862	16.6	952.4	168.3	0.0841	1.42
288.15	0.0777	17.7	897.7	205.2	0.0757	0.88
293.15	0.0662	19.4	825.0	259.8	0.0635	0.38
R32 (Difluoromethane)						
233.15	0.2115	10.4	1180.4	5.1	0.2035	17.89
243.15	0.1943	10.6	1151.2	7.7	0.1864	16.18
253.15	0.1691	10.8	1120.9	11.2	0.1612	14.40

263.15	0.1570	11.1	1089.1	15.9	0.1491	12.51
273.15	0.1453	11.4	1055.6	22.1	0.1376	10.89
283.15	0.1447	11.8	1020.0	30.2	0.1374	9.17
293.15	0.1334	12.4	981.7	40.9	0.1264	7.54
303.15	0.1310	13.0	939.9	54.8	0.1248	5.93
313.15	0.1195	13.8	893.3	73.2	0.1139	4.39
323.15	0.1117	14.7	839.7	98.4	0.1072	2.94
333.15	0.0984	15.9	774.4	135.0	0.0950	1.64
343.15	0.0812	17.4	683.4	196.8	0.0791	0.55
R125 (Pentafluoroethane)						
233.15	0.2447	10.5	1485.4	9.7	0.2392	12.29
243.15	0.2151	10.9	1447.3	14.6	0.2097	10.87
253.15	0.1930	11.4	1407.5	21.4	0.1879	9.50
263.15	0.1750	11.8	1365.4	30.4	0.1702	8.16
273.15	0.1590	12.4	1320.7	42.2	0.1548	6.83
283.15	0.1416	13.0	1272.3	57.8	0.1378	5.55
293.15	0.1314	13.7	1219.2	78.1	0.1286	4.32
303.15	0.1169	14.5	1159.4	105.0	0.1150	3.15
313.15	0.1027	15.4	1089.3	141.7	0.1019	2.05
323.15	0.0872	16.4	1001.1	195.3	0.0878	1.08
333.15	0.0661	17.7	868.3	290.7	0.0679	0.28

R143a (1,1,1-Trifluoroethane)						
253.15	0.1919	11.0	1088.4	13.7	0.1842	10.22
263.15	0.1790	11.5	1057.4	19.3	0.1714	8.81
273.15	0.1637	12.0	1024.4	26.6	0.1562	7.51
283.15	0.1509	12.6	989.1	36.1	0.1437	6.23
293.15	0.1377	13.2	950.8	48.3	0.1308	4.95
303.15	0.1283	14.0	908.5	64.1	0.1220	3.79
313.15	0.1161	15.1	860.4	85.1	0.1100	2.67
323.15	0.1036	16.4	803.5	114.1	0.0980	1.65
333.15	0.0880	17.7	729.8	158.2	0.0828	0.75
R134a (1,1,1,2-Tetrafluoroethane)						
243.15	0.3090	9.8	1388.6	4.4	0.3030	15.81
253.15	0.2671	10.2	1358.5	6.8	0.2610	14.21
263.15	0.2389	10.6	1327.4	10.0	0.2327	12.79
273.15	0.2147	11.0	1295.1	14.4	0.2085	11.43
283.15	0.1953	11.5	1261.2	20.2	0.1894	10.01
293.15	0.1781	11.9	1225.5	27.8	0.1724	8.68
303.15	0.1618	12.4	1187.6	37.5	0.1565	7.41
313.15	0.1501	12.9	1146.8	50.1	0.1455	6.04
323.15	0.1391	13.5	1102.3	66.3	0.1353	4.79
333.15	0.1265	14.2	1052.8	87.4	0.1235	3.59

343.15	0.1132	15.0	996.2	115.6	0.1113	2.47
353.15	0.0991	16.3	928.2	155.3	0.0982	1.45
363.15	0.0809	18.5	837.7	217.8	0.0798	0.57
R152a (1,1-Difluoroethane)						
243.15	0.3139	8.2	1023.1	2.6	0.3067	17.37
253.15	0.2848	8.6	1002.4	4.0	0.2773	15.87
263.15	0.2589	9.0	981.0	5.9	0.2513	14.37
273.15	0.2344	9.3	958.8	8.4	0.2267	12.98
283.15	0.2135	9.7	935.8	11.7	0.2057	11.49
293.15	0.1983	10.1	911.7	16.0	0.1907	10.15
303.15	0.1849	10.5	886.4	21.4	0.1776	8.88
313.15	0.1724	10.9	859.5	28.4	0.1654	7.58
323.15	0.1603	11.3	830.6	37.2	0.1538	6.28
333.15	0.1498	11.8	799.3	48.5	0.1441	5.05
343.15	0.1378	12.4	764.7	62.9	0.1329	3.85
353.15	0.1272	13.2	725.4	81.9	0.1234	2.74
363.15	0.1138	14.3	678.8	108.1	0.1109	1.71
373.15	0.0974	16.0	618.9	147.4	0.0947	0.81
R123 (2,2-Dichloro-1,1,1-trifluoroethane)						
253.15	0.4739	9.5	1573.8	0.9	0.4682	20.38
263.15	0.4238	9.7	1550.2	1.4	0.4179	19.30

273.15	0.3735	10.0	1526.2	2.2	0.3674	18.04
283.15	0.3380	10.3	1501.8	3.4	0.3319	16.93
293.15	0.3054	10.6	1476.8	4.9	0.2993	15.72
303.15	0.2767	10.9	1451.2	7.0	0.2705	14.48
313.15	0.2596	11.3	1425.0	9.6	0.2535	13.43
323.15	0.2377	11.6	1398.0	13.0	0.2316	12.27
333.15	0.2186	11.9	1370.1	17.3	0.2127	11.07
343.15	0.2010	12.3	1341.3	22.6	0.1953	10.04
353.15	0.1882	12.7	1311.3	29.2	0.1827	8.90
363.15	0.1757	13.2	1279.9	37.3	0.1705	7.77
373.15	0.1630	13.6	1246.9	47.0	0.1582	6.71

Table II: Coefficients of Eq. (5).

n_i', $mm^2 \cdot s^{-1}$	n_0'	$n_1' \times 10^2$	$n_2' \times 10^4$	$n_3' \times 10^7$	rms, %
R23	6.31339	-7.035036	2.692899	-3.480251	0.86
R32	5.24884	-5.105409	1.713894	-1.938356	1.63
R125	4.81031	-4.540320	1.504582	-1.707867	0.78
R143a	2.88482	-2.560307	0.824289	-0.925057	0.69
R134a	5.92848	-5.182457	1.576692	-1.633162	0.57
R152a	4.19174	-3.448395	1.007021	-1.010470	0.57
R123	6.64029	-5.147244	1.400008	-1.303028	0.79

Table III: Coefficients of Eq. (6).

	T_c, K	σ_0, mN·m^{-1}	n	rms, mN·m^{-1}
R23	298.98	61.61 ± 0.58	1.2752 ± 0.0053	0.025
R32	351.35	69.76 ± 0.84	1.2419 ± 0.0088	0.082
R125	339.33	53.59 ± 0.52	1.2638 ± 0.0068	0.040
R143a	345.89	55.77 ± 0.55	1.2877 ± 0.0063	0.028
R134a	374.18	59.69 ± 0.70	1.2656 ± 0.0088	0.055
R152a	386.41	60.24 ± 0.36	1.2525 ± 0.0047	0.046
R123	456.831	55.67 ± 0.42	1.2355 ± 0.0072	0.074

FIGURE CAPTIONS

Fig. 1 Scattering geometry.

Fig. 2 Experimental setup: optical and electronic arrangement.

Fig. 3 Kinematic viscosity of alternative refrigerants in the liquid phase under saturation conditions from surface light scattering.

Fig. 4 Surface tension of alternative refrigerants under saturation conditions from surface light scattering.

Fig. 5 Deviations of the kinematic viscosity of liquid R23 (Trifluoromethane) at saturation conditions, from Eq. (5), as a function of temperature: (▼) this work; (·····) Latini et al. [30]; (◇) Geller [18]; (⋈) Phillips and Murphy [29].

Fig. 6 Deviations of the kinematic viscosity of liquid R32 (Difluoromethane) at saturation conditions, from Eq. (5), as a function of temperature: (▼) this work; (– · –) Grebenkov et al. [34]; (□) Heide [33]; (·····) Latini et al. [30]; (×) Sun et al. [32]; (– –) Assael et al. [36]; (+) Oliveira and Wakeham [19]; (⬭) Ripple and Matar [31]; (△) Sagaidakova et al. [35].

Fig. 7 Deviations of the kinematic viscosity of liquid R125 (Pentafluoroethane) at saturation conditions, from Eq. (5), as a function of temperature: (▼) this work; (□) Heide [33]; (·····) Latini et al. [30]; (×) Sun et al. [32]; (– –) Assael et al. [36]; (▽) Diller and Peterson [37]; (+) Oliveira and Wakeham [19]; (○) Ripple and Matar [31]; (⊠) Wilson et al. [38].

Fig. 8 Deviations of the kinematic viscosity of liquid R143a (1,1,1-Trifluoroethane) at saturation conditions, from Eq. (5), as a function of temperature: (▼) this work; (□) Heide [33]; (·····) Latini et al. [30]; (⊠) Kumagai and Takahashi [39].

Fig. 9 Deviations of the kinematic viscosity of liquid R134a (1,1,1,2-Tetrafluoroethane) at saturation conditions, from Eq. (5), as a function of temperature: (▼) this work; (– · –) Grebenkov et al. [34]; (□) Heide [33]; (·····) Latini et al. [30]; (– –) Assael et al. [36]; (▽) Diller et al. [40]; (——) Krauss et al. [20]; (+) Oliveira and Wakeham [41]; (○) Ripple and Matar [31]; (⊠) Kumagai and Takahashi [39].

Fig. 10 Deviations of the kinematic viscosity of liquid R152a (1,1-Difluoroethane) at saturation conditions, from Eq. (5), as a function of temperature: (▼) this work; (– · –) Grebenkov et al. [34]; (□) Heide [33]; (——) Krauss et al. [21]; (·····) Latini et al. [30]; (– –) Assael et al. [36]; (○) van der Gulik [27]; (⊠) Kumagai and Takahashi [39]; (△) Sagaidakova et al. [35].

Fig. 11 Deviations of the kinematic viscosity of liquid R123 (2,2-Dichloro-1,1,1-trifluoroethane) at saturation conditions, from Eq. (5), as a function of temperature: (▼) this work; (·····) Latini et al. [30]; (▽) Diller et al. [40]; (– · ·) Tanaka and Sotani [42]; (⊠) Kumagai and Takahashi [39].

Fig. 12 Deviations of the surface tension of R23 (Trifluoromethane) at saturation conditions, from Eq. (6), as a function of temperature: (▼) this work; (– · ·) Le Neindre and Garrabos [45]; (——) Okada and Watanabe [44]; (□ ·····) Heide [43].

Fig. 13 Deviations of the surface tension of R32 (Difluoromethane) at saturation conditions, from Eq. (6), as a function of temperature: (▼) this work; (□ ·····) Heide [46]; (○ ——) Okada and Higashi [47]; (– –) Schmidt and Moldover [49]; (⊠ – · –) Zhu and Lu [48].

Fig. 14 Deviations of the surface tension of R125 (Pentafluoroethane) at saturation conditions, from Eq. (6), as a function of temperature: (▼) this work; (□ ·····) Heide [46]; (○ ——) Okada and Higashi [47]; (– –) Schmidt and Moldover [49].

Fig. 15 Deviations of the surface tension of R143a (1,1,1-Trifluoroethane) at saturation conditions, from Eq. (6), as a function of temperature: (▼) this work; (□ ·····) Heide [46]; (——) Srinivasan and Oellrich [14]; (– –) Schmidt et al. [50].

Fig. 16 Deviations of the surface tension of R134a (1,1,1,2-Tetrafluoroethane) at saturation conditions, from Eq. (6), as a function of temperature: (▼) this work; (□ ·····) Heide [46]; (△ – –) Chae et al. [52]; (+ – · ·) Sufen et al. [53]; (——) Okada and Higashi [28]; (– · –) Zhu et al. [54]; (– – ·) Higashi and Okada [55].

Fig. 17 Deviations of the surface tension of R152a (1,1-Difluoroethane) at saturation conditions, from Eq. (6), as a function of temperature: (▼) this work; (□ ·····) Heide [46]; (○ ——) Okada and Higashi [47]; (+ – · ·) Sufen et al. [53]; (– – ·) Higashi and Okada [55]; (– –) Chae et al. [56]; (– · –) Obata from Okada and Higashi [28].

Fig. 18 Deviations of the surface tension of R123 (2,2-Dichloro-1,1,1-trifluoroethane) at saturation conditions, from Eq. (6), as a function of temperature: (▼) this work; (——) Okada and Higashi [28]; (– – ·) Higashi and Okada [55]; (△ – –) Chae et al. [52].

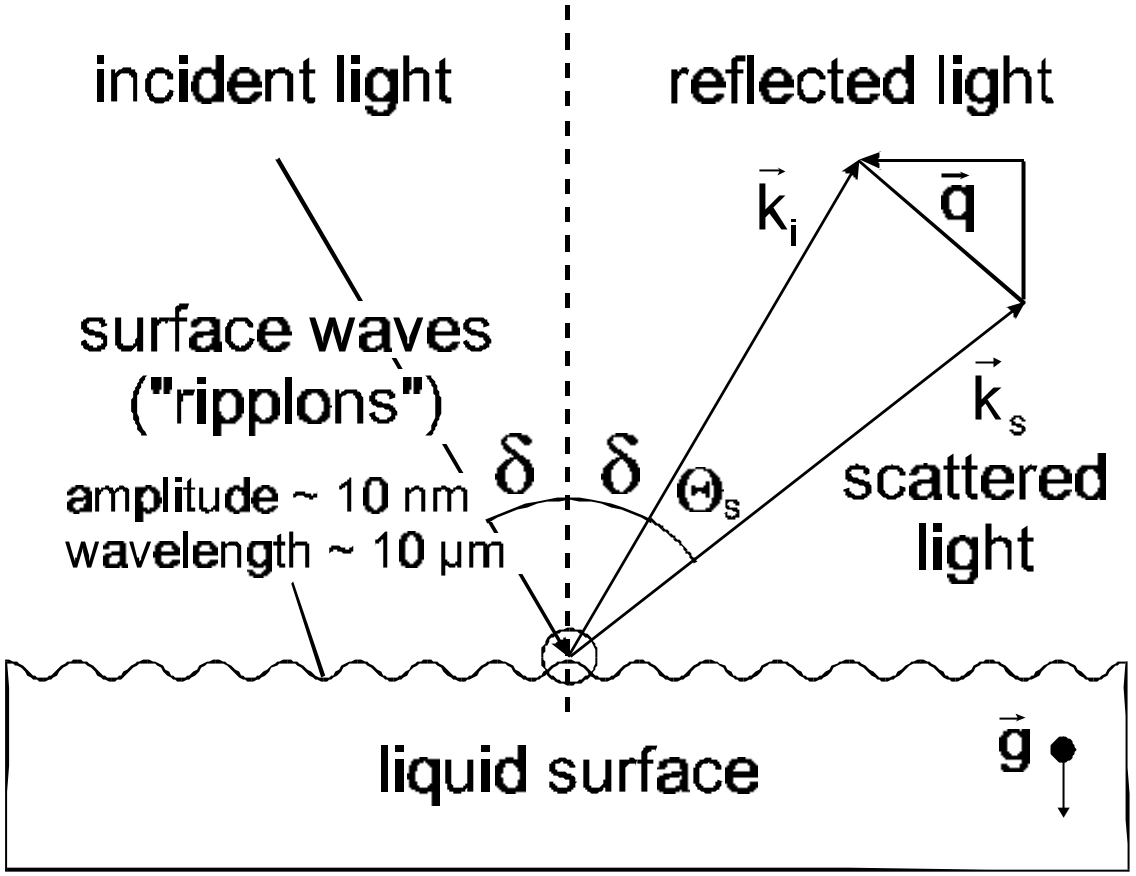

Fröba, Will, and Leipertz, Fig. 1

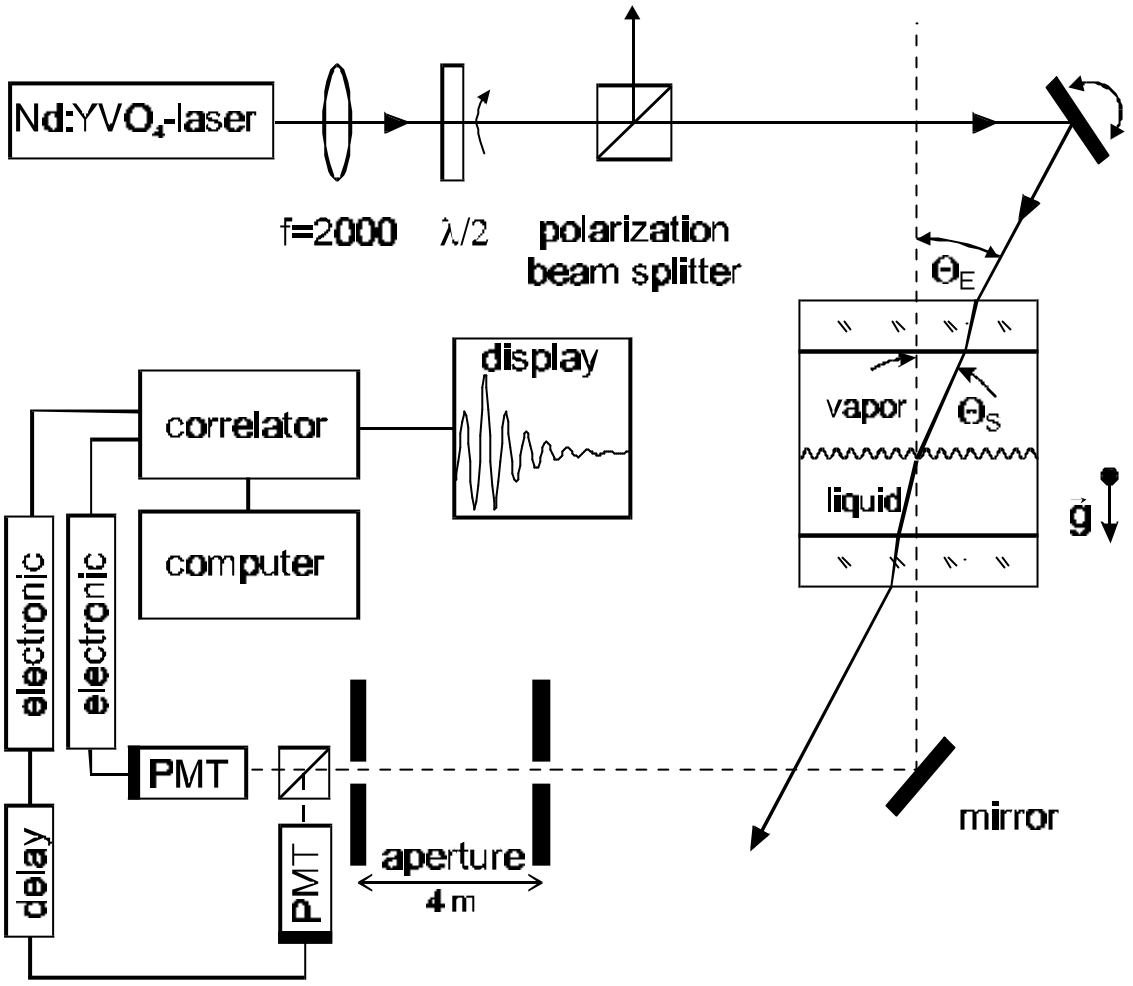

Fröba, Will, and Leipertz, Fig. 2

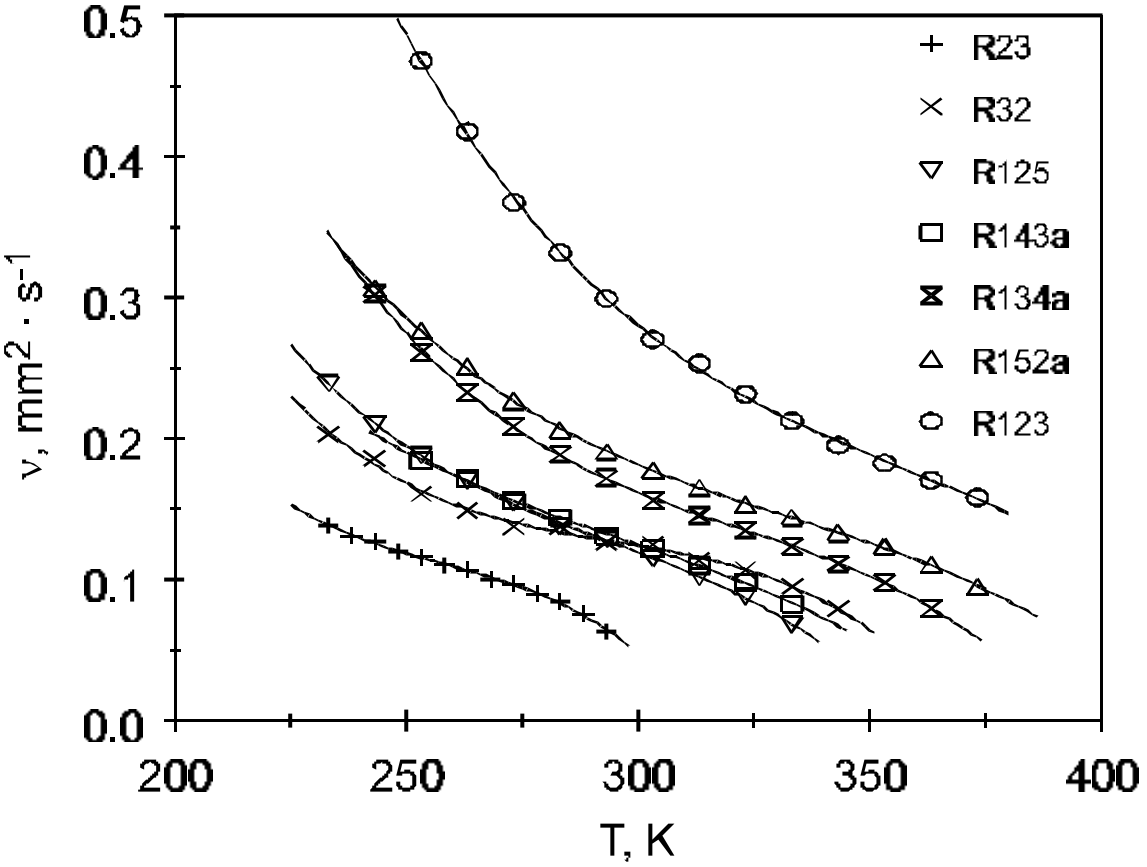

Fröba, Will, and Leipertz, Fig. 3

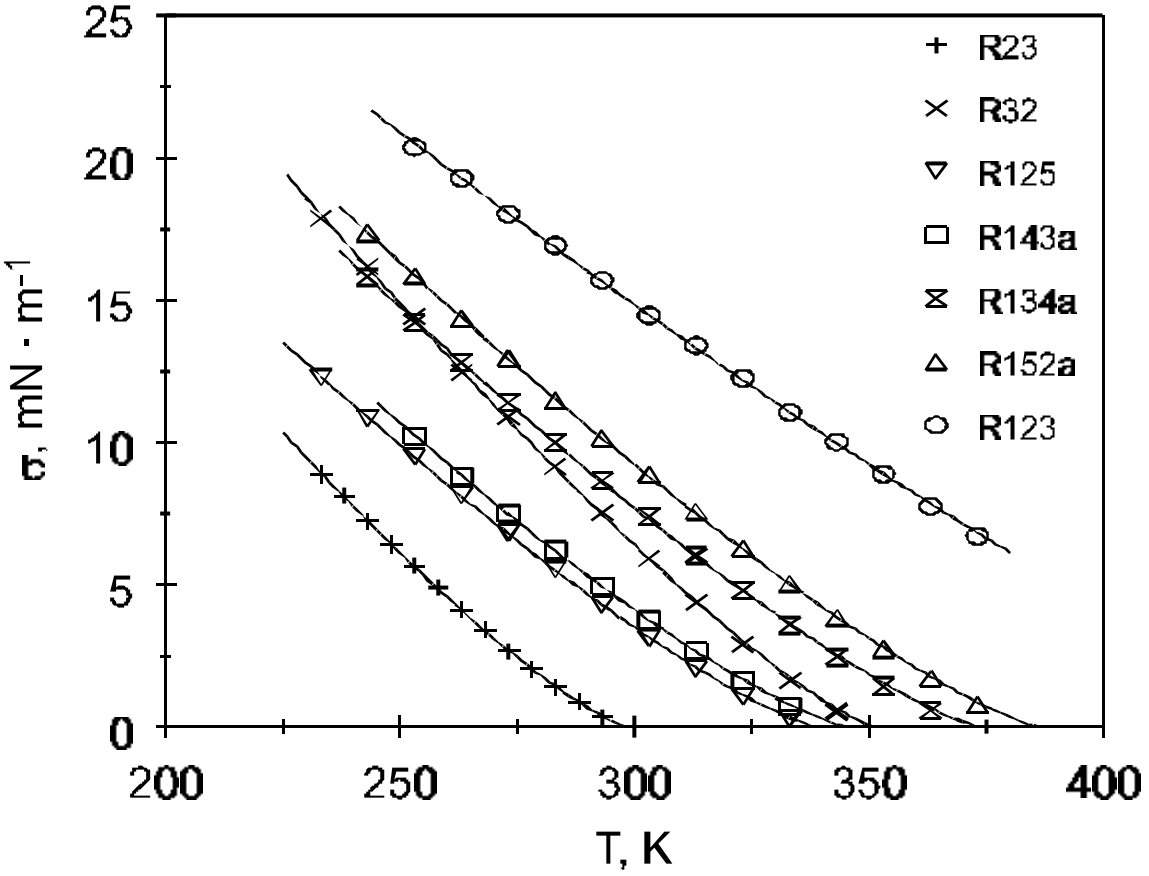

Fröba, Will, and Leipertz, Fig. 4

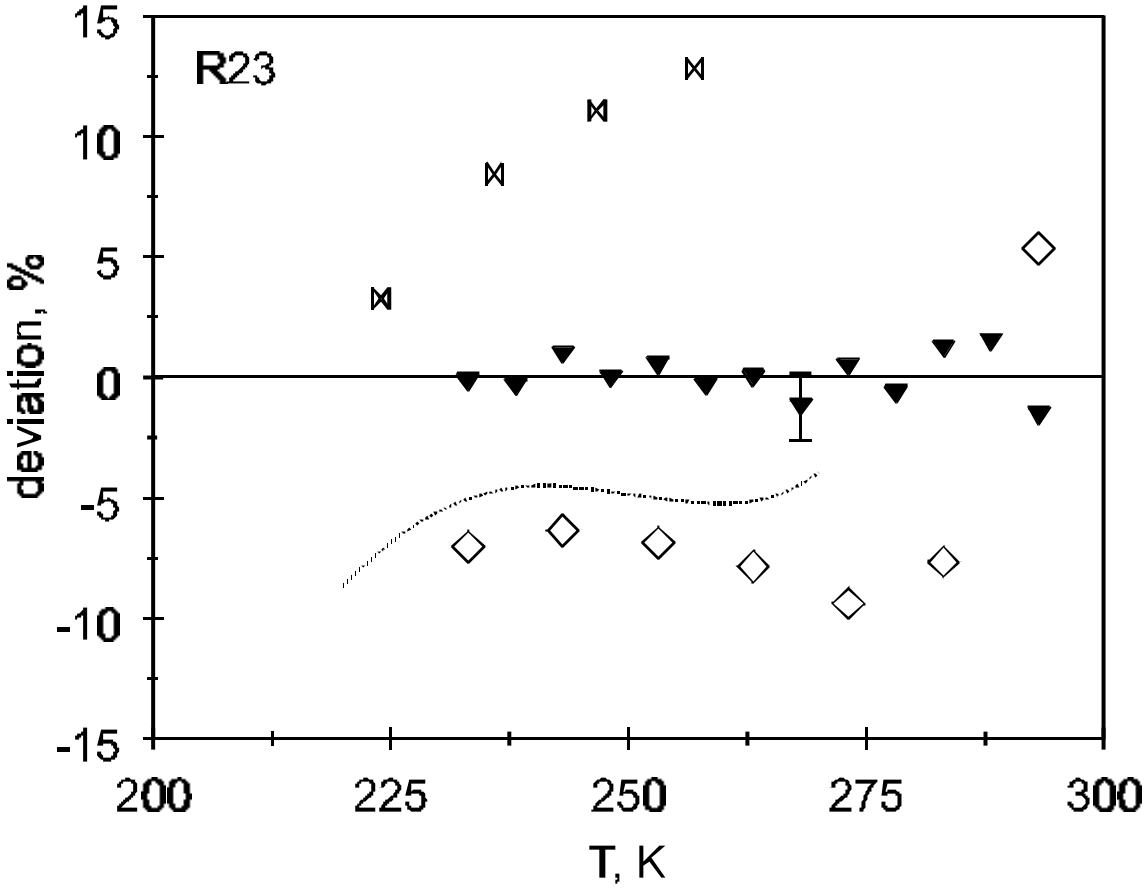

Fröba, Will, and Leipertz, Fig. 5

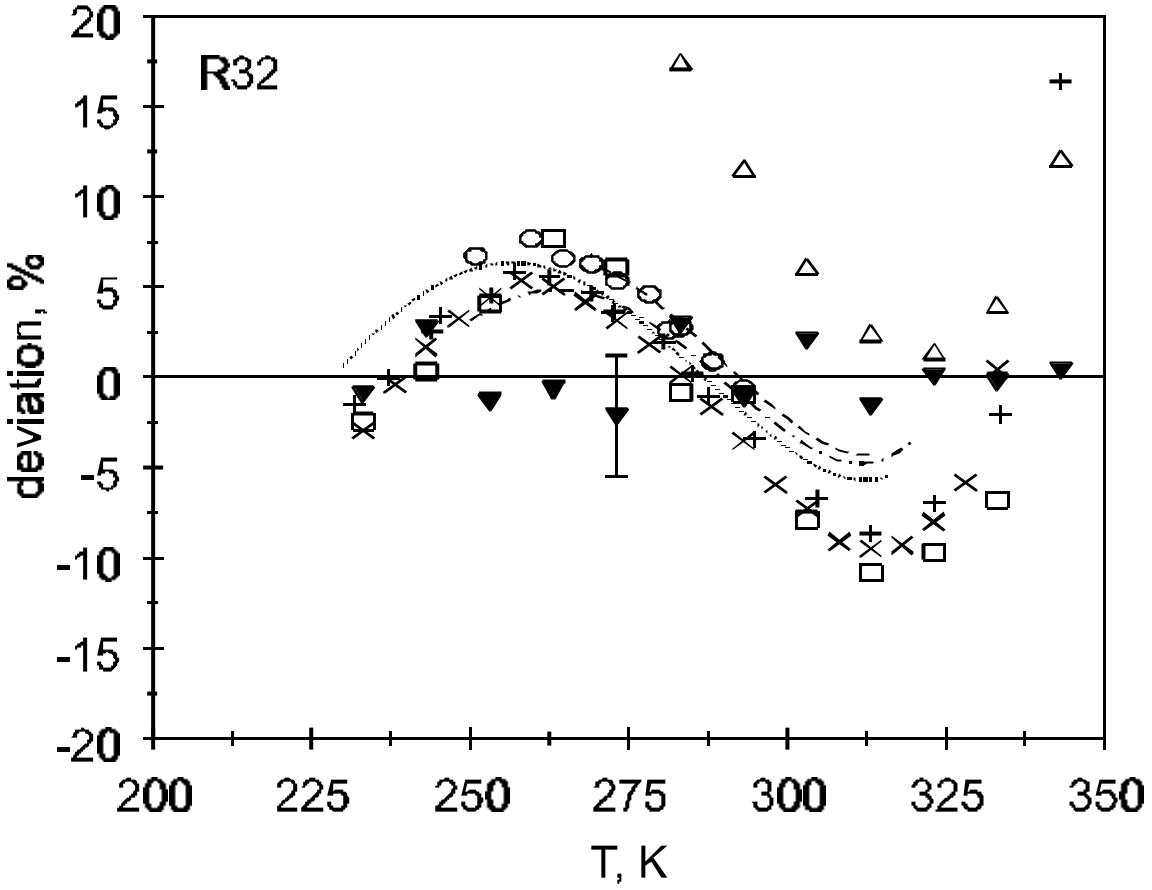

Fröba, Will, and Leipertz, Fig. 6

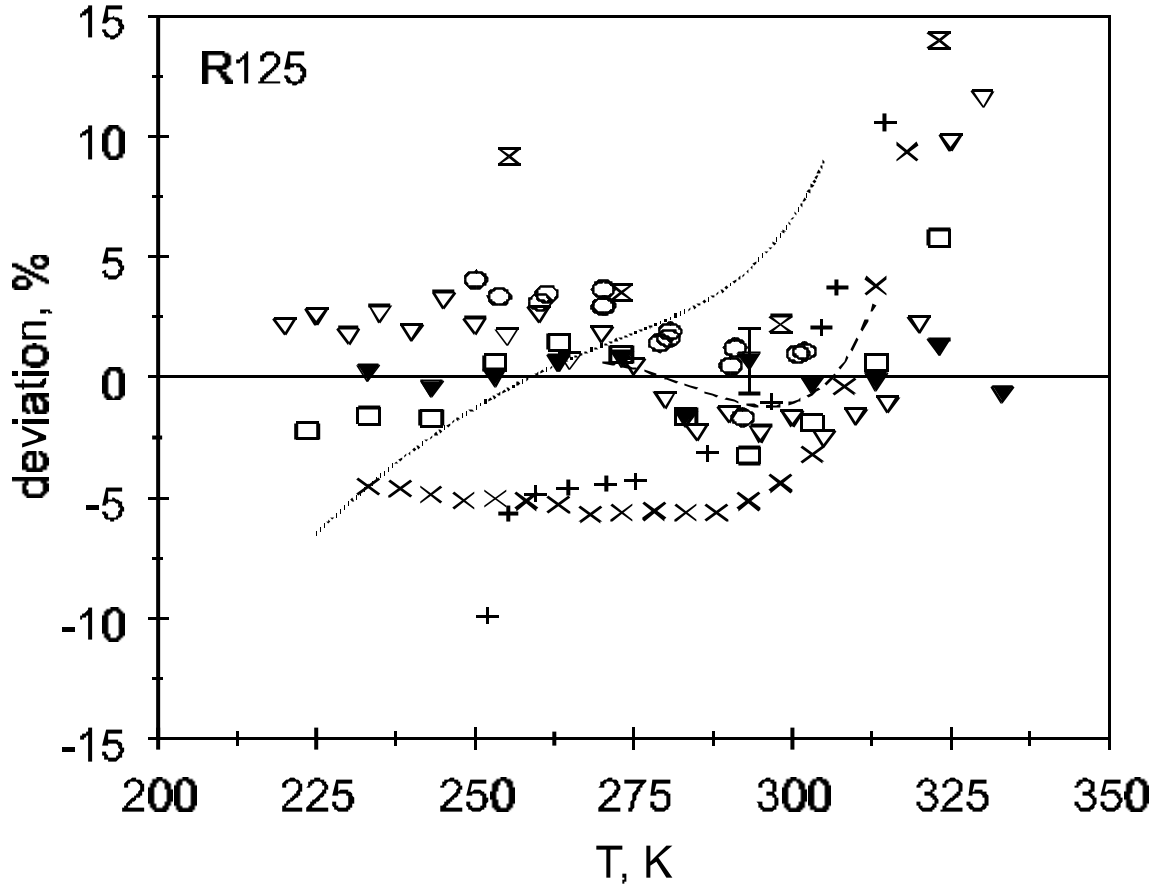

Fröba, Will, and Leipertz, Fig. 7

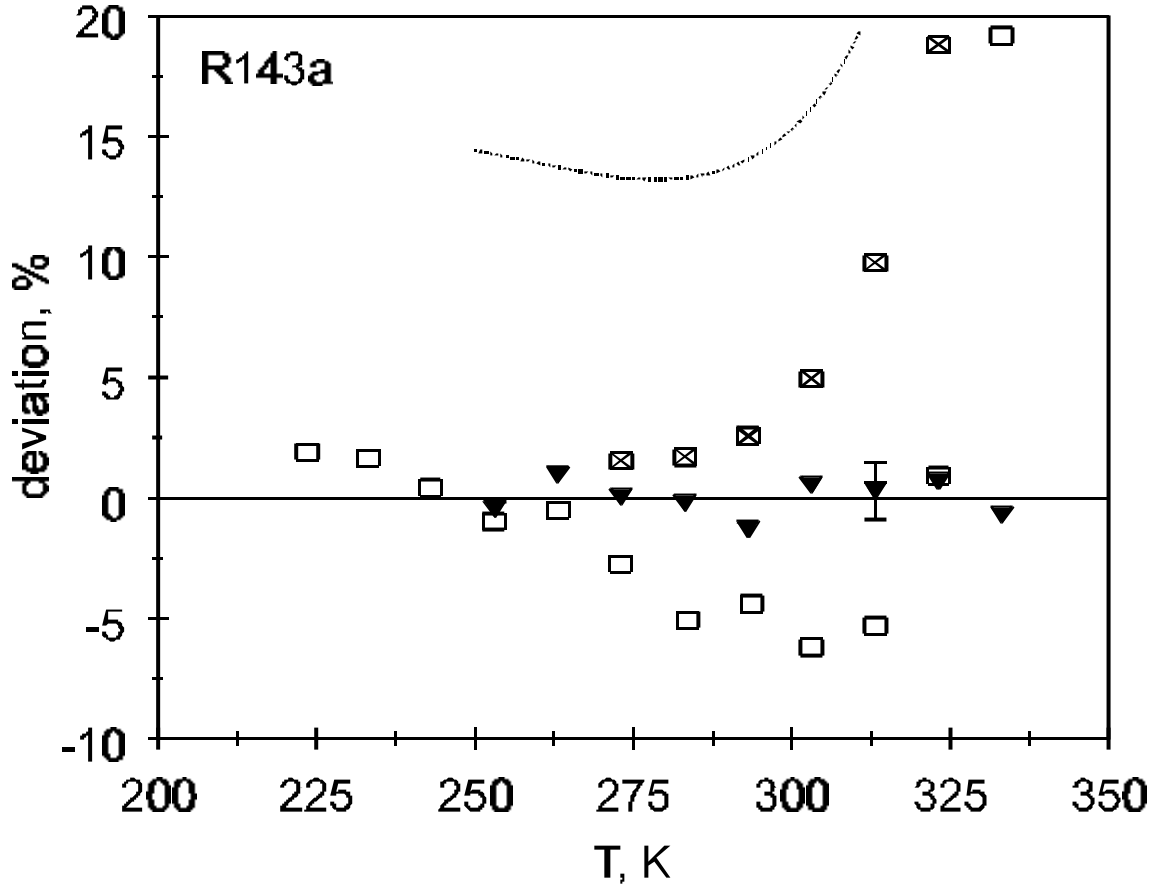

Fröba, Will, and Leipertz, Fig. 8

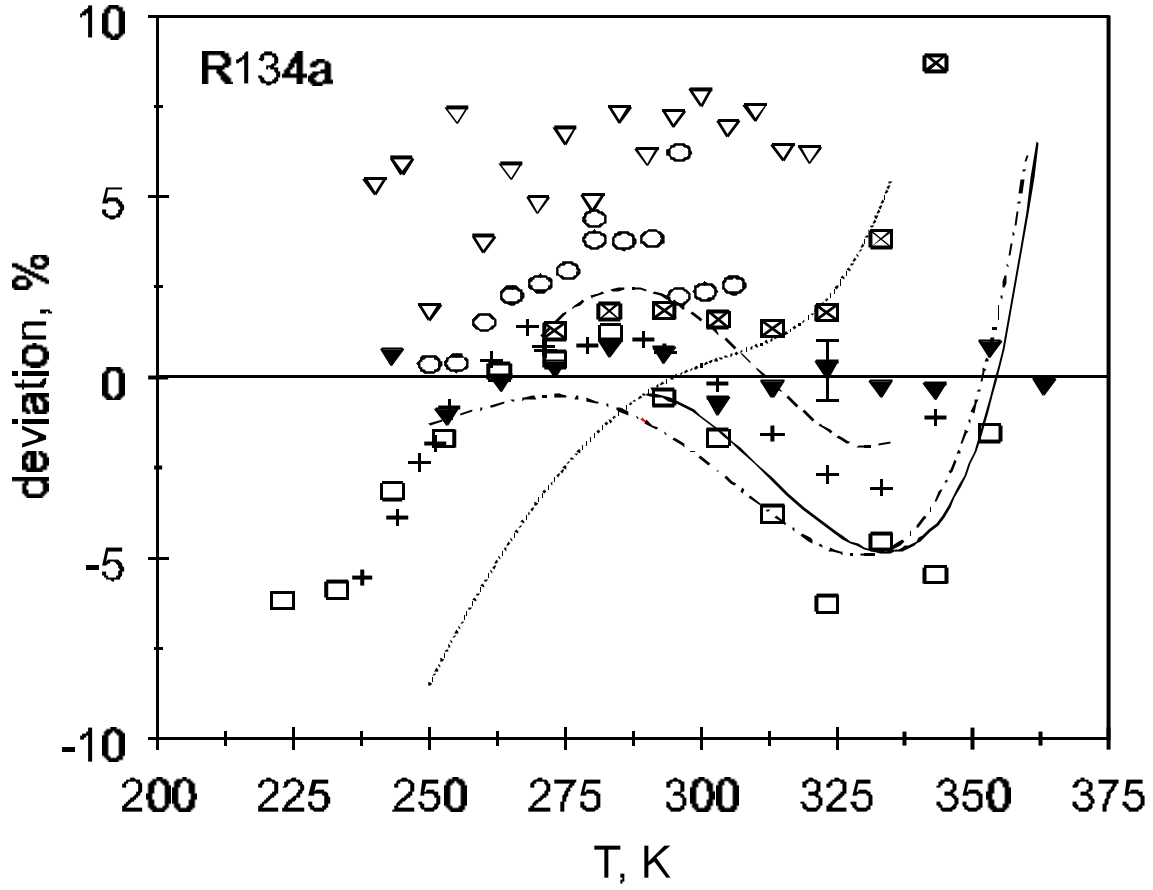

Fröba, Will, and Leipertz, Fig. 9

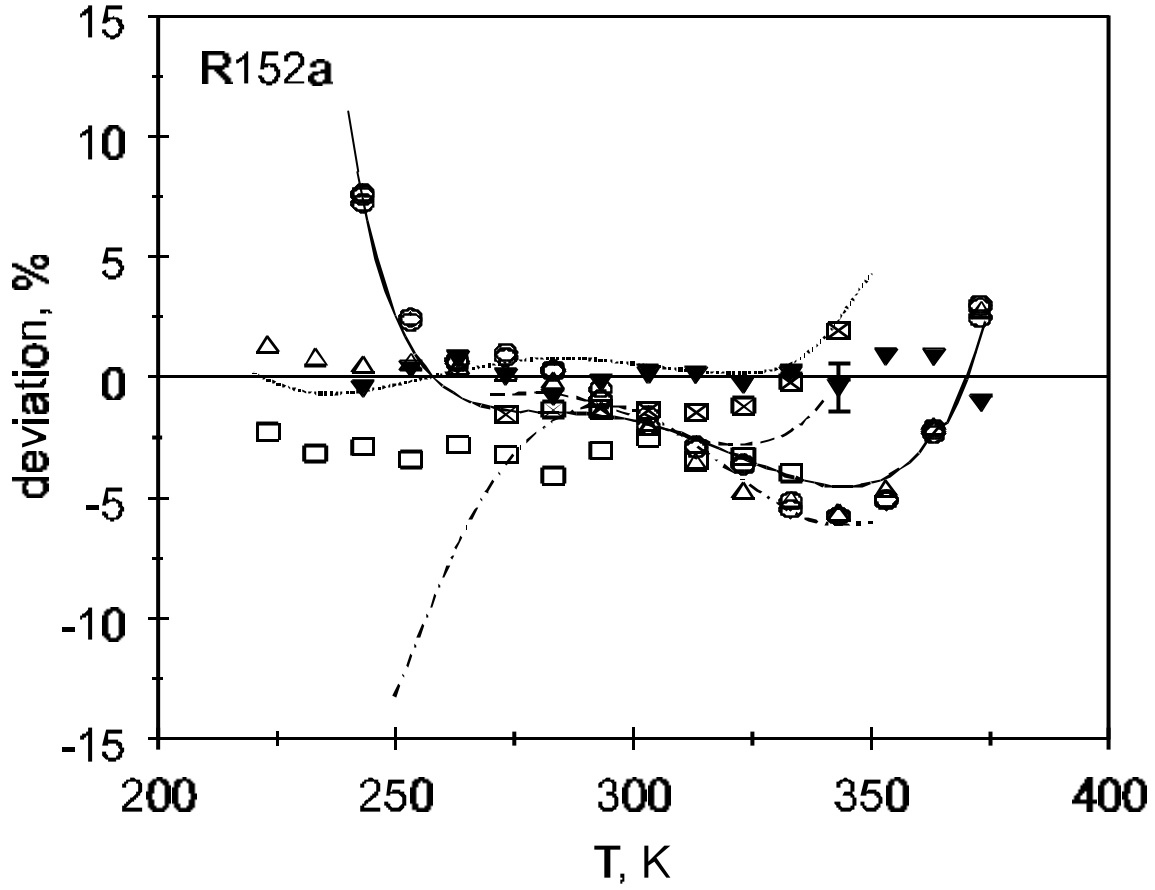

Fröba, Will, and Leipertz, Fig. 10

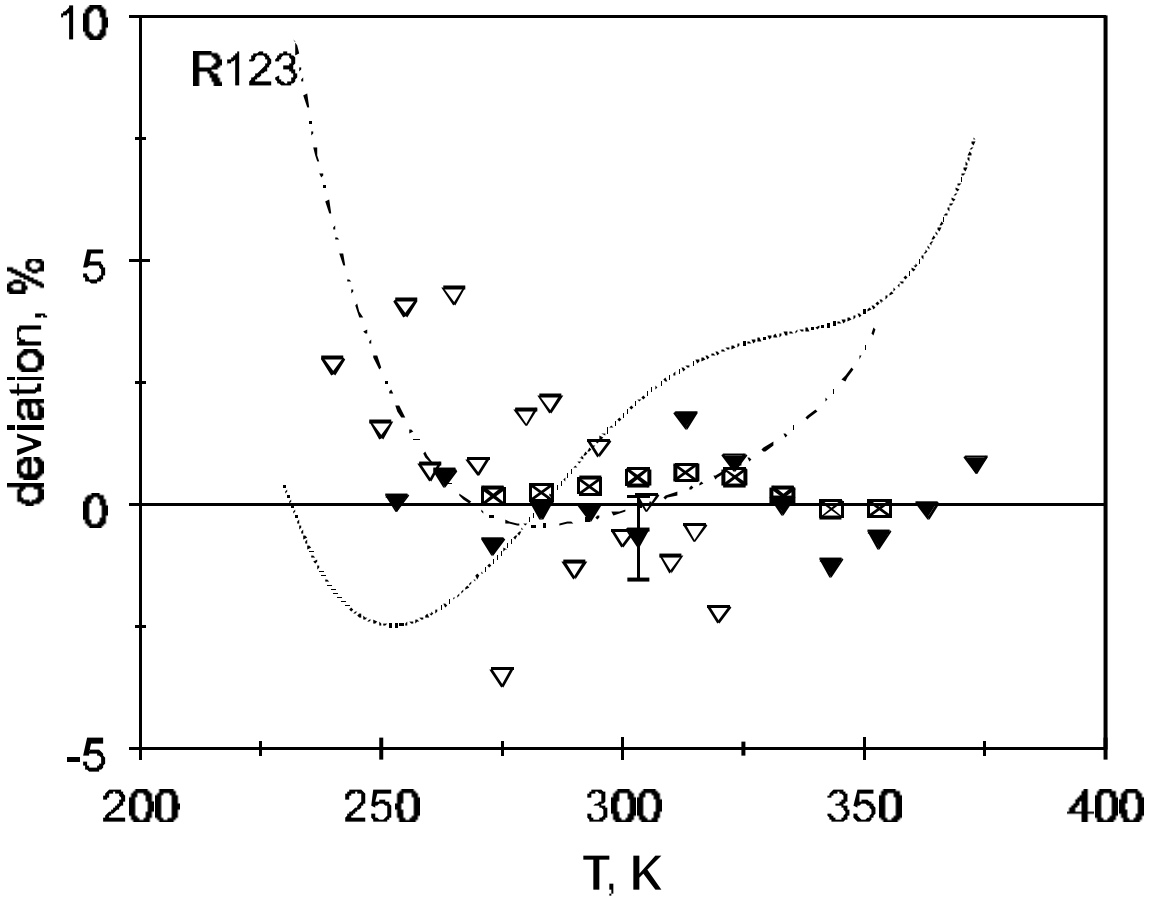

Fröba, Will, and Leipertz, Fig. 11

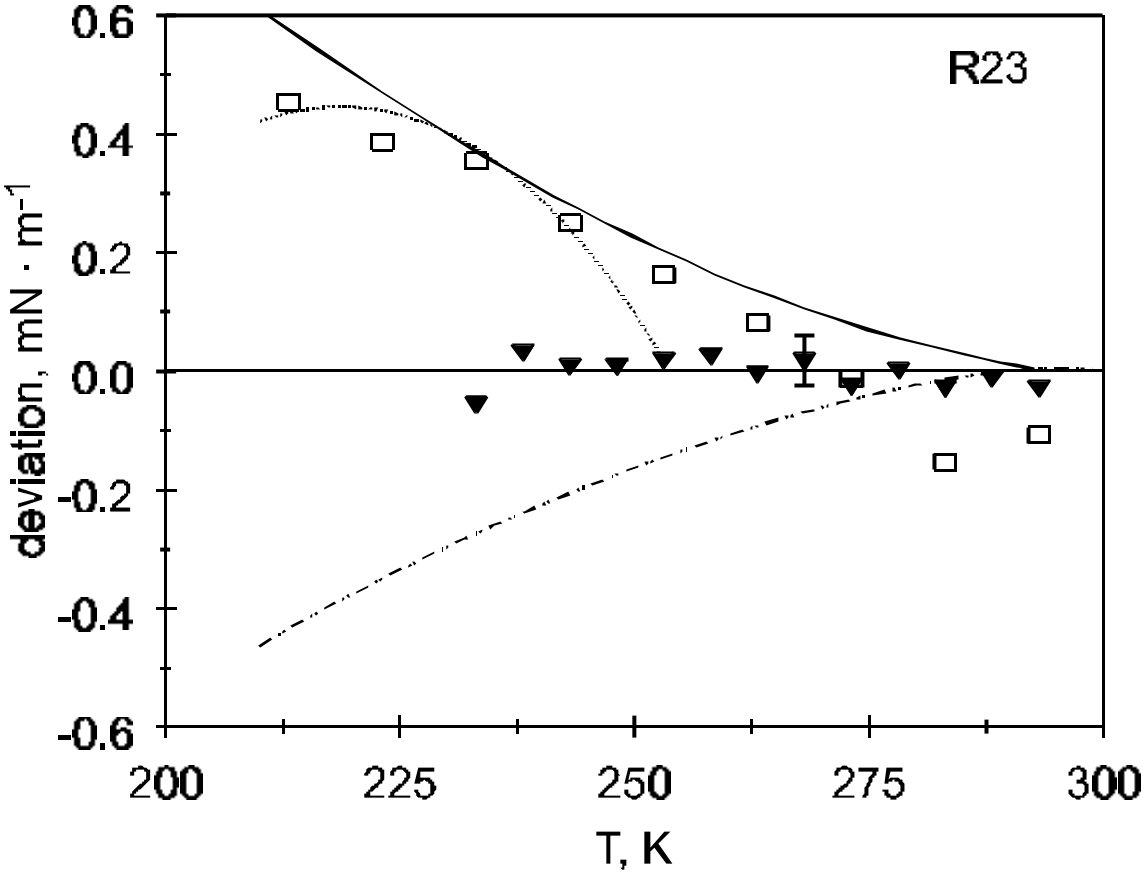

Fröba, Will, and Leipertz, Fig. 12

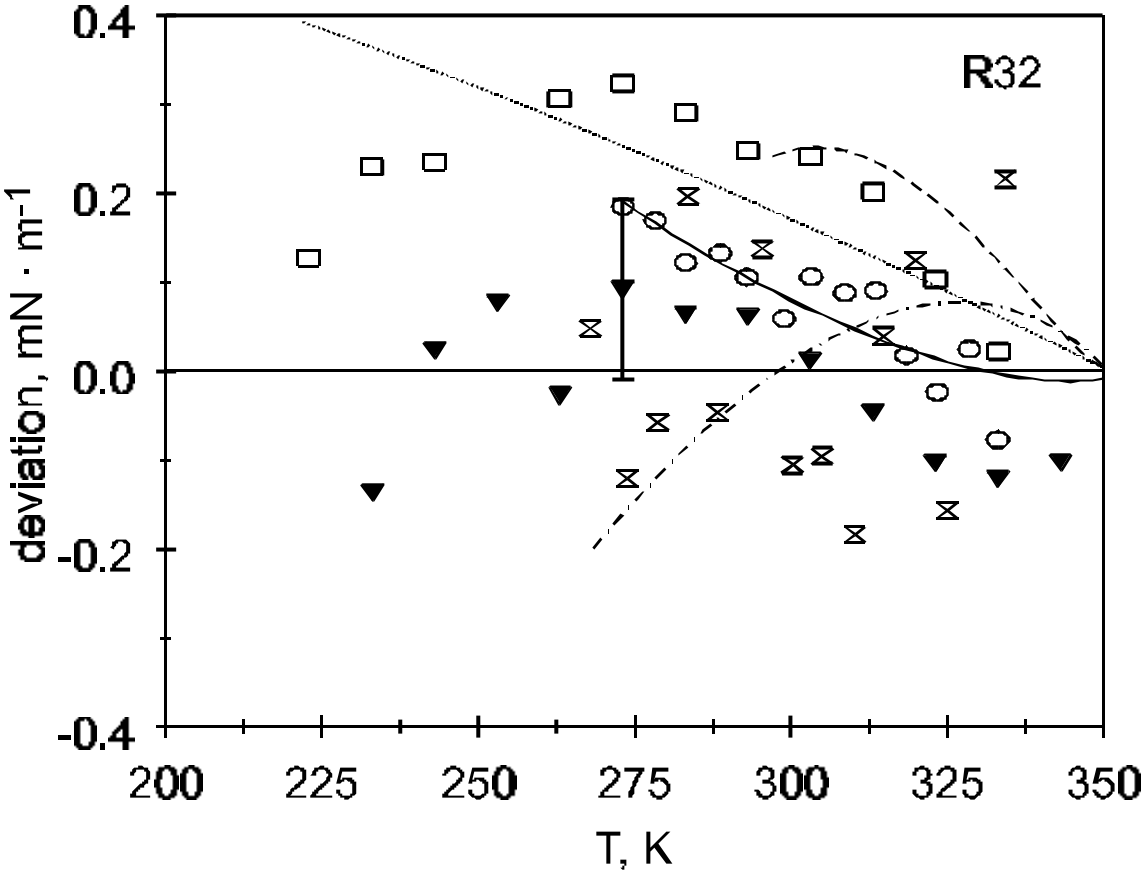

Fröba, Will, and Leipertz, Fig. 13

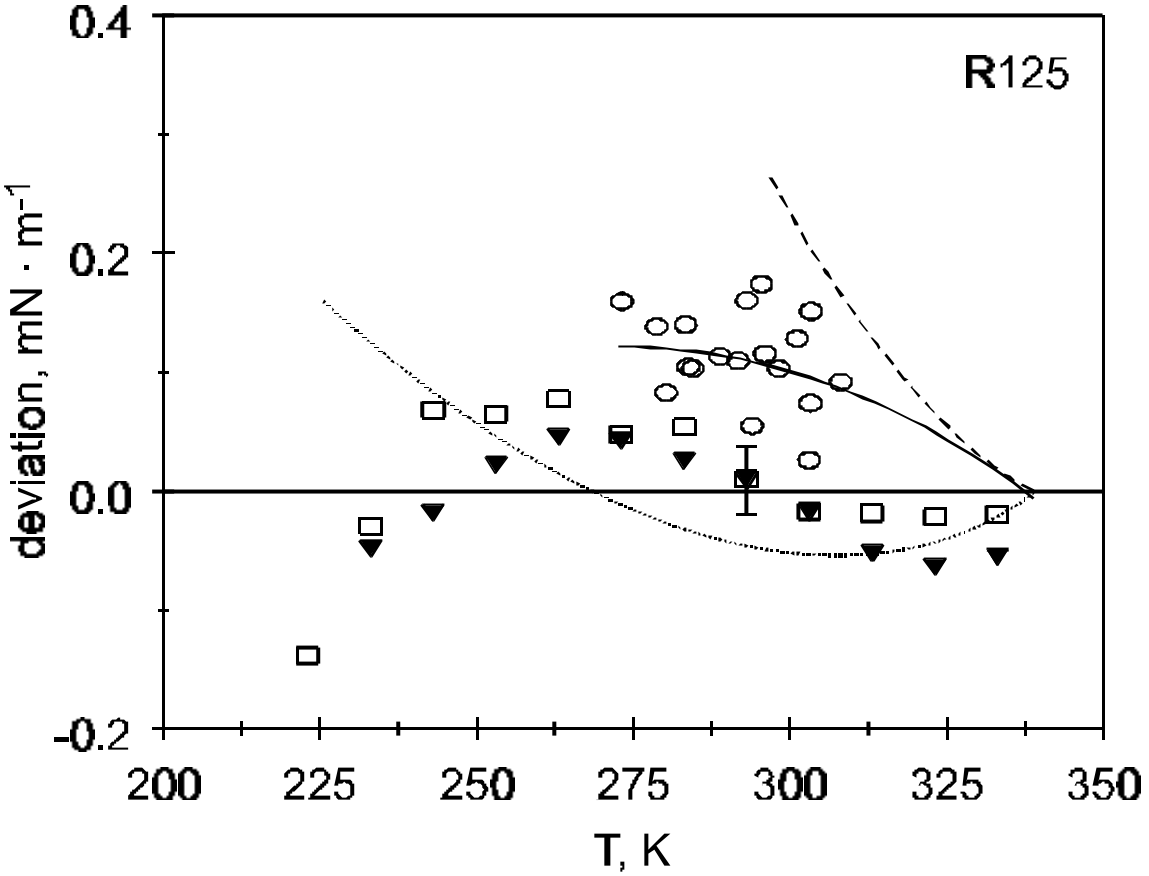

Fröba, Will, and Leipertz, Fig. 14

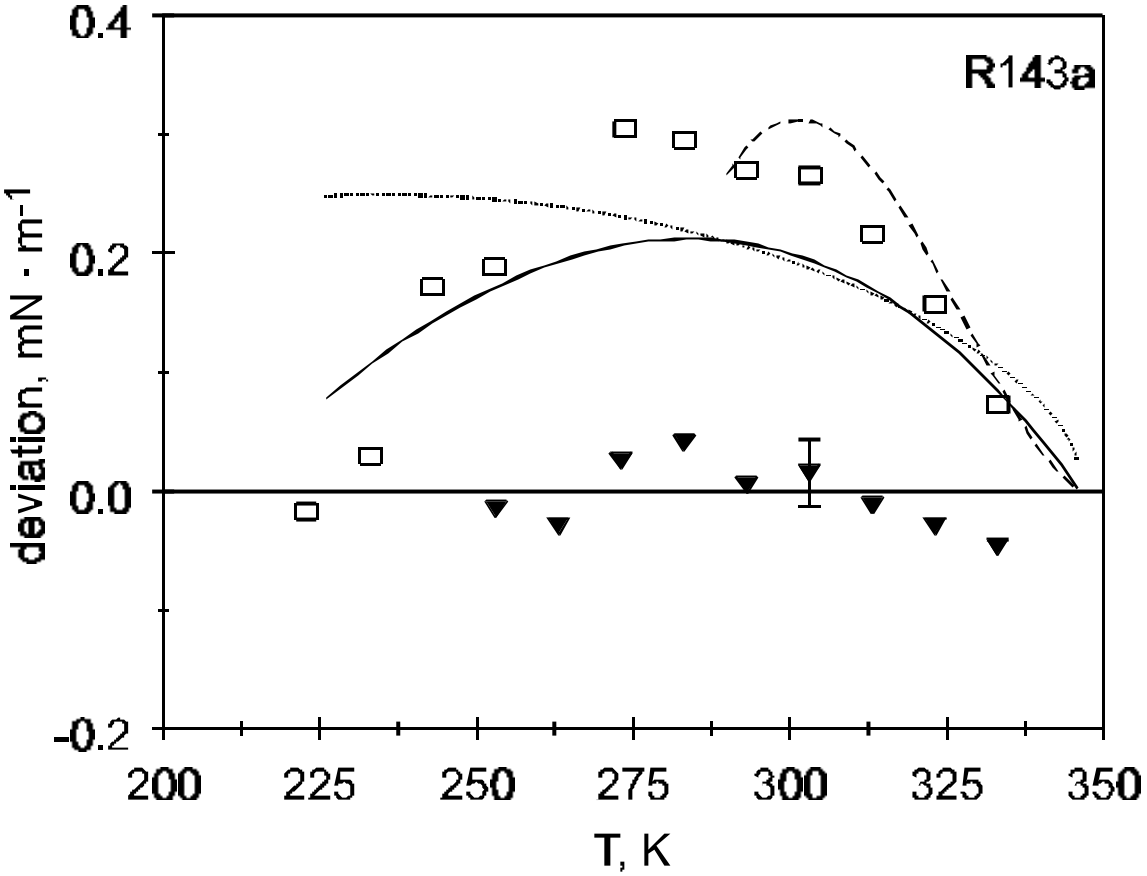

Fröba, Will, and Leipertz, Fig. 15

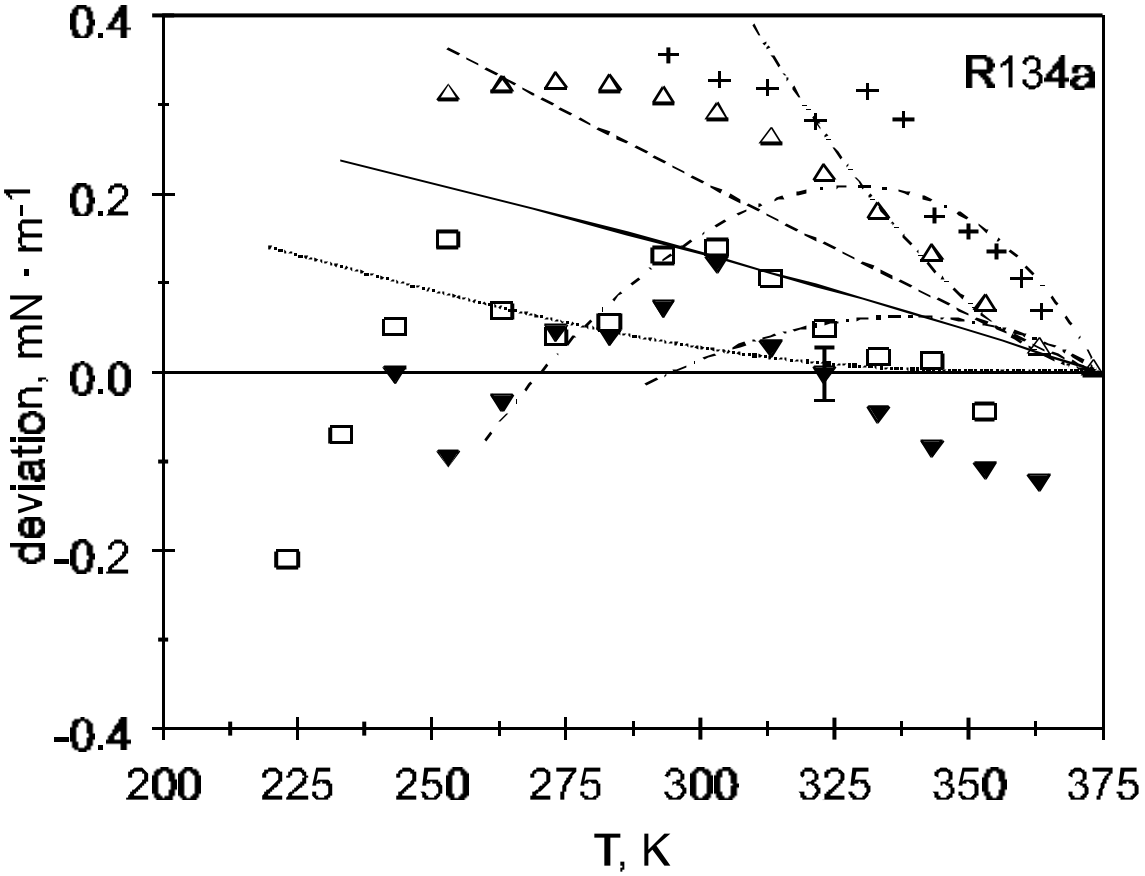

Fröba, Will, and Leipertz, Fig. 16

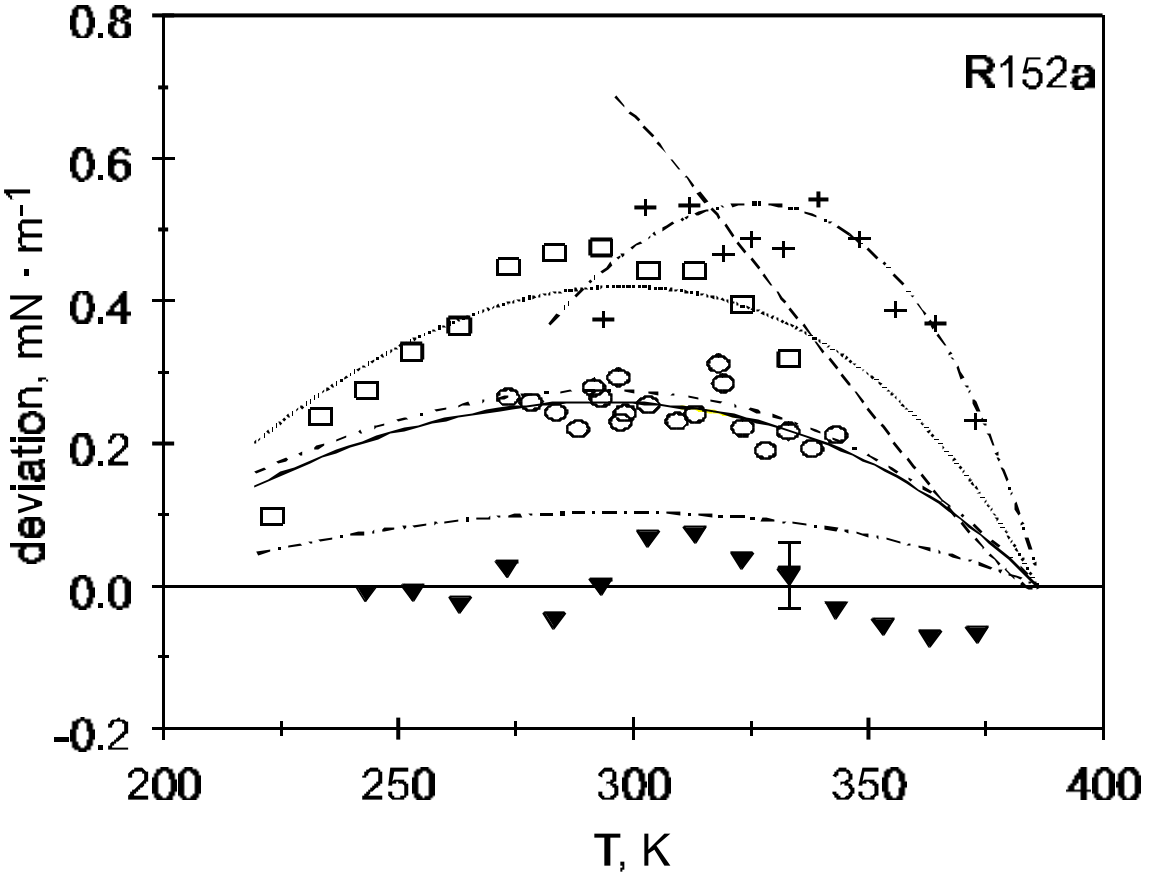

Fröba, Will, and Leipertz, Fig. 17

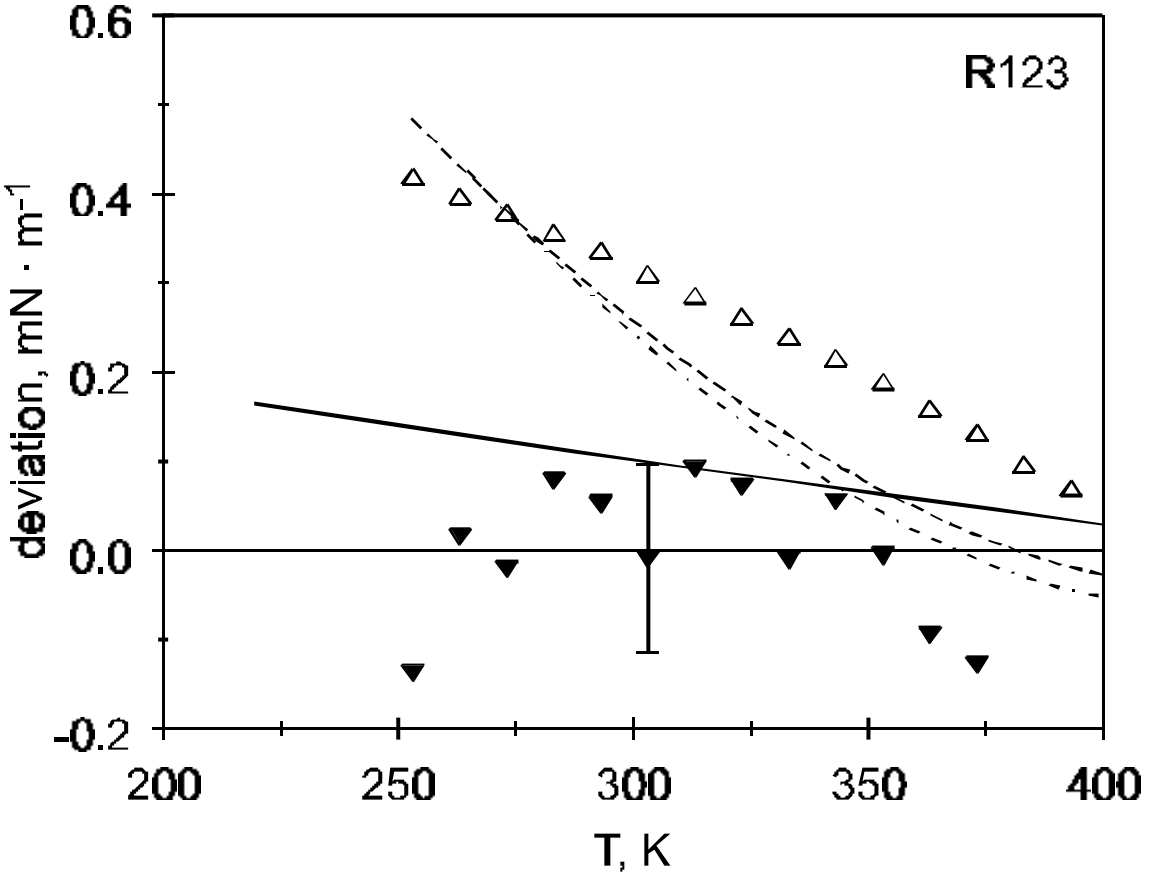

Fröba, Will, and Leipertz, Fig. 18